Molecular-Recognition-Directed Self-Assembly of Supramolecular Polymers

V. Percec[a]; J. Heck[a]; G. Johansson[a]; D. Tomazos[a]; M. Kawasumi[a]; G. Ungar[b]

[a] Department of Macromolecular Science, Case Western Reserve University, Cleveland, Ohio, USA [b] Department of Engineering Materials and Centre for Molecular Materials, The University of Sheffield, Sheffield, UK

PLEASE SCROLL DOWN FOR ARTICLE

MOLECULAR-RECOGNITION-DIRECTED SELF-ASSEMBLY OF SUPRAMOLECULAR POLYMERS

V. PERCEC,* J. HECK, G. JOHANSSON, D. TOMAZOS, and M. KAWASUMI

Department of Macromolecular Science
Case Western Reserve University
Cleveland, Ohio 44106, USA

G. UNGAR

Department of Engineering Materials and Centre for Molecular Materials
The University of Sheffield
Sheffield, S1 DU, UK

ABSTRACT

The first part of this paper discusses the molecular design of se-lected examples of structural units containing taper-shaped *exo*-receptors and various crown ether, oligooxyethylenic, and H-bonding-based *endo*-receptors, which self-assemble into cylindrical channel-like architectures via principles resembling those of tobacco mosaic virus. The ability of these structural units to self-assemble via a delicate combination of *exo*- and *endo*-recognition processes will be presented. A comparison between various *supramolecular* (generated via H-bonding, ionic, and electro-static interactions) and *molecular "polymer backbones"* will be made. The present limitations concerning the ability to engineer the structural parameters of these supramolecular channel-like architectures and some possible novel material functions derived from them will be briefly men-tioned. The second part of this paper discusses our research on the molecular design of a novel class of macrocyclics which self-assemble via intramolecular recognition processes into supramolecular "rodlike" collapsed macrocyclics which display thermotropic liquid crystalline

mesophases. It is demonstrated that these macrocyclics have a higher ability to form liquid crystalline phases than the corresponding linear compounds which have identical or even higher degrees of polymerization. Therefore, they represent the ideal molecular architectures which generate mesophases.

INTRODUCTION

For the past 150 years organic chemists have been concerned mainly with understanding the covalent bond. Recently, research on molecular recognition (generated by weak, noncovalent interactions) has been recognized worldwide as an important intellectual and technological frontier [1]. *Endo-* (generated by convergent cavities) and *exo-* (generated by larger bodies of similar size and shapes, or surfaces) molecular recognition [2], preorganization, and self-organization provide the basis of spontaneous generation of functional supramolecular architectures via self-assembly from their components (Scheme 1) [3]. Molecular-recognition-directed organic synthesis or self-synthesis [4] and self-assembly of supramolecular architectures [2, 3] are two of the most active topics of supramolecular chemistry [2a]. It is well accepted that molecular-recognition-directed synthesis and self-

MOLECULAR RECOGNITION

ENZYMES ◄─────────┬──── ENDO - RECOGNITION (RECEPTORS)
                    │   - i.e. convergent cavities - cyclophanes
                    │   like crown - ethers (inclusion complexes)

PROTEIN - PROTEIN   ◄──── EXO - RECOGNITION (RECEPTORS)
ANTIBODY - ANTIGEN   - i.e. external surfaces or bodies of
INTERACTIONS   similar size

                      PREORGANIZATION

SELF-ASSEMBLY ─────────────► TRANSITION STATE

Molecular Recognition   Molecular Recognition
Directed Self-Assembly   Directed ORGANIC
of SUPRAMOLECULAR   SYNTHESIS OR SELF-
ARCHITECTURES   SYNTHESIS

SUPRAMOLECULAR ASSEMBLIES

SCHEME 1.   Supramolecular chemistry pathways.

assembly are responsible for the generation and the fascinating properties of biological systems. The goal of this paper is to discuss recent progress on two topics under investigation in our laboratory, i.e., molecular design of supramolecular architectures which self-assemble via principles which resemble that of tobacco mosaic virus (TMV) and macrocyclic liquid crystals.

Toward Tobacco Mosaic Virus-Like Self-Assembled Supramolecular Architectures

TMV represents the best understood self-assembled biological system [3a, 3b, 5]. Therefore, we believe it provides an ideal model to be used for an understanding of the principles governing the self-assembly of synthetic supramolecular architectures.

Synthetic Strategy Used in the Design of TMV-Like Supramolecular Architectures

TMV is a simple virus consisting only of a single type of protein molecule and of a strand of ribonucleic acid (RNA), the carrier of genetic information. Figure 1 provides a simplified picture of its self-assembly. Its single rod-shape results from its design, namely a regular helical array of 2130 identical protein molecules (or subunits) in which is embedded a single molecule of RNA. The virus dimensions are 3000 Å in length, 180 Å in diameter, a helical pitch of 23 Å, and a central hole of 40 Å. TMV self-assembles upon mixing of its individual components. Therefore, it is considered that all the information necessary to assemble TMV is contained in its components, i.e., mostly within the protein subunits. Under certain pH conditions the proteins self-assemble into a TMV even in the absence of RNA. Therefore, either RNA or pH can initiate the conformational change of a double or single layered disk from its disklike shape into a lock-washer shape which is responsible for the generation of the single helix of TMV. The first driving force toward this self-assembled system is provided by the *exo*-recognition of the tapered shapes of the proteins. *Exo*-recognition makes use of an external surface, and the *exo*-receptor substrate binding occurs by surface-to-surface interaction [2a]. Therefore, *exo*-recognition with strong selective binding requires a large enough contact area and a sufficient number of interactions as well as geometrical and site complementarity between the two surfaces. Consequently, *exo*-recognition includes recognition between large bodies of similar size as well as recognition at interfaces. Protein-protein and antibody–antigen interactions occur via an *exo*-recognition process while enzymes function via an *endo*-recognition process [2a]. Consequently, the first step toward a TMV-like self-assembly consists of the design of synthetic organic molecules having a specific tapered shape which resembles that of the proteins from Fig. 1. Lipids are classic molecules whose shape is determined by the number of chains and the ratio between their head and tail diameters [6]. In addition, they self-assemble into spherical and cylindrical micelles and bilayer structures whose architectures are determined by the shape of the lipid (Fig. 2). The shape of the lipid can be manipulated via temperature and the amount of water of hydration. At higher concentrations, cylindrical micelles self-assemble into a hexagonal columnar mesophase, spherical micelles self-assemble into a cubic mesophase, while layered

a)

Viral RNA

$d = 40\ \text{Å}$
$D = 180\ \text{Å}$
$L/D = 16.6$
pitch = 23 Å

$L = 3000\ \text{Å}$

Tobacco Mosaic Virus

b)

c)

limited stacks of disks   crystal

single helix

single helix

"lock-washer"

disk

disk

disk

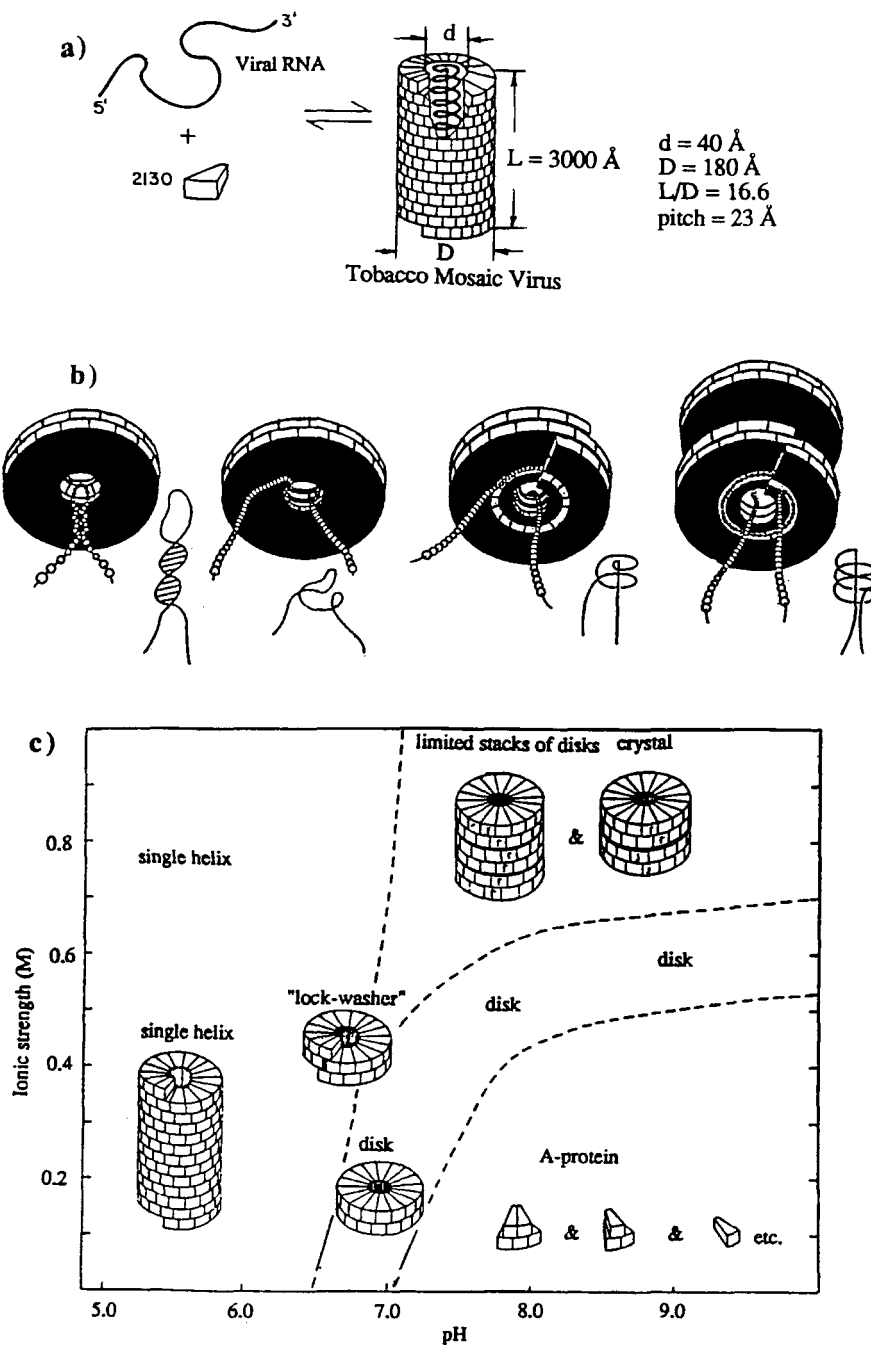A-protein

&   &   etc.

Ionic strength (M)

pH

FIG. 1. The assembly of the tobacco mosaic virus: (a) from its constituent protein subunits and viral RNA into a cylindrically shaped tubular supramolecule; (b) the threading of the RNA in a hairpin conformation into a double layered disk of protein subunits initiating the change to a lock-washer conformation; (c) the dependence of the self-assembly of the protein subunits on pH (adapted from Refs. 3a, 5, and 10).
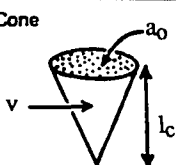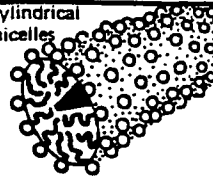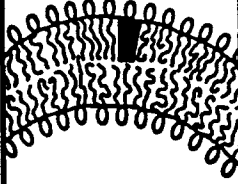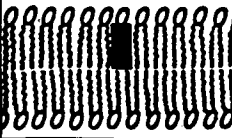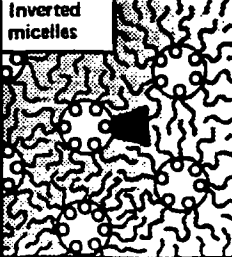
Lipid	Critical packing parameter $v/a_o l_c$	Critical packing shape	Structures formed
Single-chained lipids with large head-group areas	$< 1/3$	Cone	Spherical micelles
Single-chained lipids with small head-group areas	$1/3 - 1/2$	Truncated cone	Cylindrical micelles
Double-chained lipids with large head-group areas, fluid chains	$1/2 - 1$	Truncated cone	Flexible bilayers, vesicles
Double-chained lipids with small head-group areas	~ 1	Cylinder	Planar bilayers
Double-chained lipids with small head-group areas	> 1	Inverted truncated cone or wedge	Inverted micelles

FIG. 2. The dependence of the shape of lipids on the structures which they self-assemble into: a_o = optimal head group area; l_c = critical chain length; v = volume of hydrocarbon chains (adapted from Ref. 6).

structures assemble into lamellar mesophases [7]. Therefore, at a different scale, the self-assembly of the cylindrical micelles of lipids resembles the self-assembling of the constituent proteins of TMV. The simplest nonamphiphilic homologue of lipids with a tapered shape can be designed by the alkylation of alkyl 3,4,5-trihydroxybenzoate with either bromoalkanes or alkoxybenzyloxybenzyl chloride. Variants of these taper-shaped side groups were attached to polymer backbones either via polymer homologues [8] or by polymerization [9, 10] reactions. The resulting polymers self-assemble into cylindrical architectures which generate a columnar hexagonal (Φ_h) liquid crystalline phase. These preliminary experiments have demonstrated that various substituted gallic acid derivatives can be used to construct *exo*-receptors with a tapered shape.

   This paper will review some of our efforts directed toward the molecular design of TMV-like supramolecular architectures via synthetic strategies consisting of various combinations of molecular and supramolecular chemistries.

SUPRAMOLECULAR CYLINDERS BY A COMBINATION OF *ENDO-* AND *EXO-*RECOGNITION

Crown Ethers as *Endo*-Receptors

   Crown ethers are a class of *endo*-receptors containing an endohydrophilic cavity ideally suited for the binding of positively charged substrates. The binding ability of crown ethers is controlled by a number of factors including the size of the macrocycle, the number of donor atoms present in the cycle, its conformational flexibility, and the electronic effects of substituents present on the macrocycle. We have demonstrated that by taking all these factors into consideration, it is possible to design highly selective *endo*-receptors based on crown ethers that can ultimately facilitate the self-assembly of various supramolecular architectures.

   For the present study, two crown ether *endo*-receptors have been employed. Their synthesis has been reported previously [11, 12] and is outlined in Fig. 3. In the first case the conformationally rigid 4′-hydroxymethyl(benzo-15-crown-5) (**B15C5**) *endo*-receptor was employed. In the second case the more conformationally flexible (±)-hydroxymethyl(15-crown-5) (**15C5**) *endo*-receptor was used. No thermodynamic data for complexes of **15C5** and **B15C5** with sodium cations under comparable conditions are available in the literature. However, stability constants (log K_s), where $K_S = k_{complexation}/k_{decomplexation}$ ($k_{complexation}$ and $k_{decomplexation}$ are the rate constants for complexation and decomplexation, respectively) can be determined from solution ionic conductivity. Correspondingly, log K_S for complexation of **15C5** (log K_s = 2.70) [13] and banxo-15-crown-5 (log K_s = 2.68) [14] with sodium cations in 90% aqueous MeOH solution, where conformational effects are minimized, are nearly identical. Therefore, any differences in the phase behavior of self-assembled complexes derived from structural units containing **15C5** and **B15C5** *endo*-receptors should result from differences in the conformational flexibility of the two macrocycles and not from differences in their electronic nature.

   The facile esterification of **B15C5** or **15C5** with 3,4,5-tris(*p*-dodecyloxybenzyloxy)benzoic acid (**12-ABG**) resulted in the taper-shaped structural units **12-ABG-B15C5** and **12-ABG-15C5**, respectively, which contain one of the two crown ethers as *endo*-receptors and **12-ABG** as the *exo*-receptor (Fig. 3). The esterification of
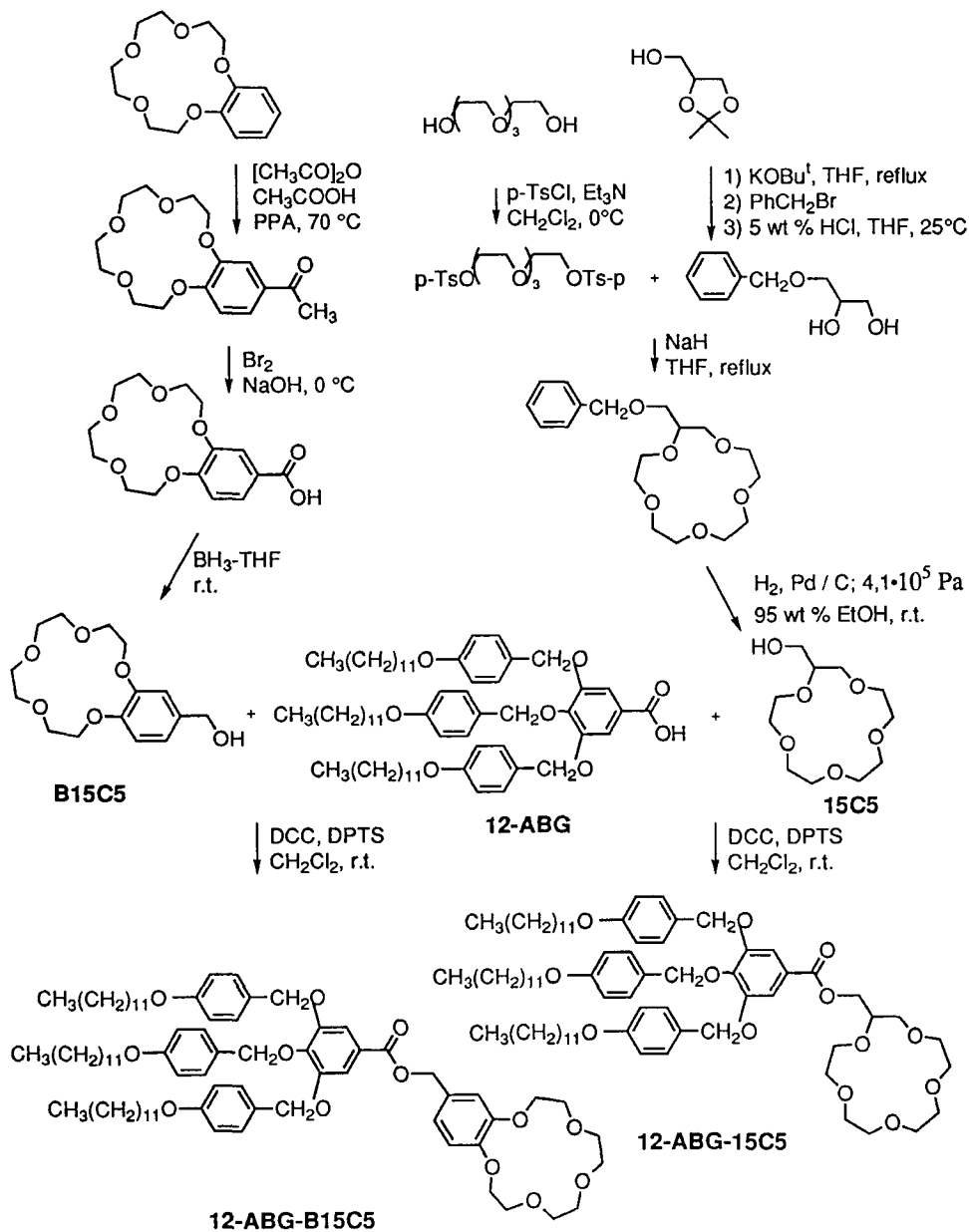
FIG. 3. Synthesis of **12-ABG-B15C5** and **12-ABG-15C5** building blocks. (PPA = polyphosphoric acid; p-TsCl = p-toluene sulfonyl chloride; THF = tetrahydrofuran; DDC = dicyclohexylcarbodiimide; DPTS = N,N-dimethylaminopyridinium p-toluenesulfonate.)

15C5 with 3,4,5-tris(*p*-dodecyloxy)benzoic acid (**12-AG**) yielded a shorter taper-shaped structural unit, **12-AG-15C5**, which lacks the benzyl ether moieties in the alkyl tails of its *exo*-receptor. The phase behavior of **12-ABG-B15C5**, **12-ABG-15C5**, and **12-AG-15C5** and of their complexes with sodium triflate (NaOTf) and potassium triflate (KOTf) was investigated by a combination of techniques consisting of differential scanning calorimetry (DSC), thermal optical polarized microscopy, and small- (SAXS) and wide-angle x-ray scattering (WAXS), and was already discussed in detail [8–11].

The structure of **12-ABG-B15C5** is shown in Fig. 4(a). Figures 4(b) and 4(c) presents the DSC thermograms from the second heating scan of the complexes of **12-ABG-15C5** with NaOTf and KOTf, respectively. For further elucidation, the
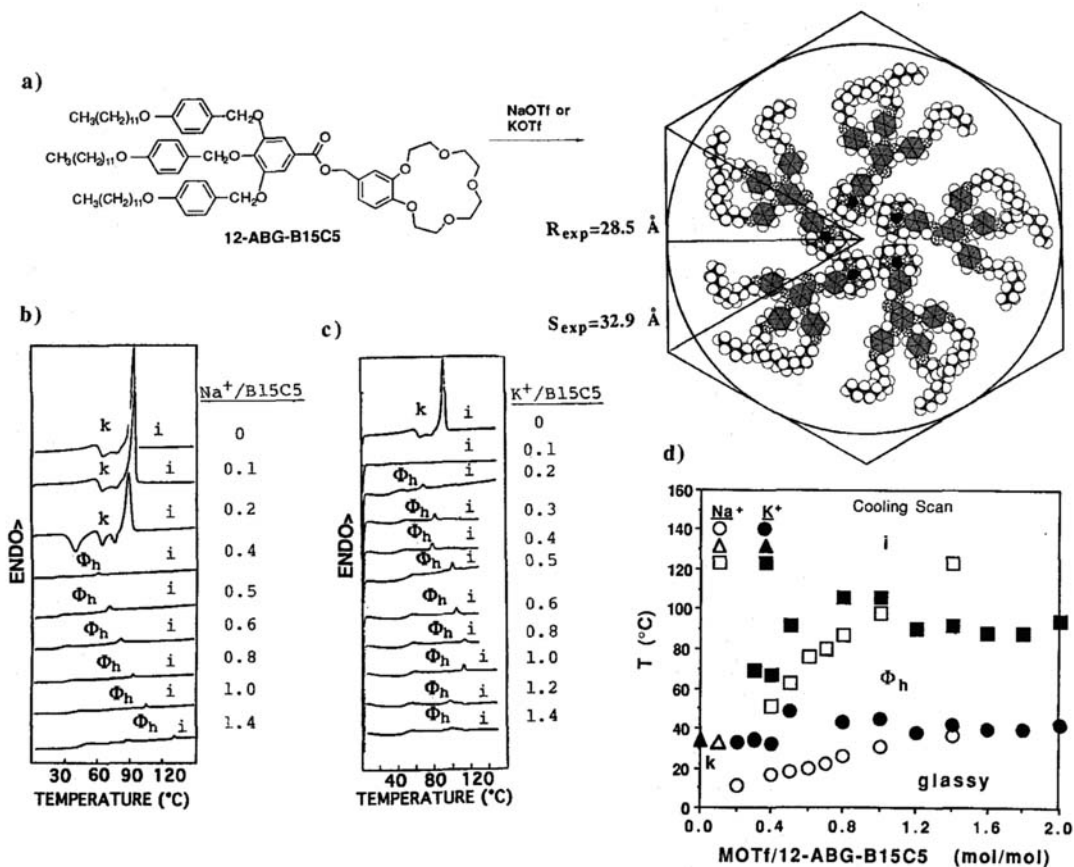
FIG. 4. Schematic representation of a cross section of the supramolecular column formed upon complexation of **12-ABG-B15C5** with sodium triflate (NaOTf) or potassium triflate (KOTf). (a) Representative DSC traces (second heating scans, 20°C/min) of the complexes of **12-ABG-B15C5** with NaOTf (b) and with KOTf (c). (d) The dependence of the transition temperatures of the complexes of **12-ABG-B15C5** with MOTf on the MOTf/**12-ABG-B15C5** molar ratio determined during the first DSC cooling scans. M = Na: (○) T_g; (△) T_{i-k}; (□) $T_{i-\Phi h}$. M = K: (●) T_g; (▲), T_{i-k}; (■) $T_{i-\Phi h}$.

dependence of the transition temperatures of **12-ABG-B15C5** and its complexes with NaOTf and KOTf determined by DSC during the first cooling scans are plotted in Fig. 4(d).

The uncomplexed tapered structural unit, **12-ABG-B15C5**, is crystalline and melts into an isotropic liquid at 96°C. Its crystalline phase obtained after fresh recrystallization from solution or melt displays a number of sharp small- and wide-angle reflections corresponding to a lamellar crystalline structure. Complexation of **12-ABG-B15C5** with less than 0.3 moles of NaOTf per **B15C5** decreases its crystallization ability. However, complexation of **12-ABG-B15C5** with as little as 0.4 mole NaOTf per mole **B15C5** results in spontaneous self-assembly of a hexagonal columnar (Φ_h) mesophase at a temperature $T > T_g$ (T_g = glass transition temperature). The presence of a T_g on the DSC trace of this complex suggests a cooperative motion which is characteristic for polymer systems. Focal conic or fan-shaped textures, which are representative of Φ_h mesophases, were observed by optical polarized microscopy. Increasing the amount of NaOTf results in an increase in the isotropic-Φ_h transition temperature ($T_{i-\Phi h}$). The complex of **12-ABG-B15C5** with as much as 1.8 moles NaOTf per mole **12-ABG-B15C5** exhibited a Φ_h mesophase. However, at this concentration of NaOTf, the sample was subject to Lewis-acid-catalyzed decomposition by NaOTf at temperatures higher than 120°C.

Complexation of **12-ABG-B15C5** with as little as 0.1 mole KOTf per mole **B15C5** (Fig. 4c) results in a glassy compound while its complexation with 0.2 moles KOTf results in the spontaneous self-assembly of a Φ_h mesophase. For comparison, in the case of the complexes of **12-ABG-B15C5** with NaOTf, the formation of a Φ_h mesophase required 0.4 mole salt. This shows that a salt based on a larger cation induces the formation of a Φ_h mesophase in **12-ABG-B15C5** at lower concentrations. Furthermore, complexes of **12-ABG-B15C5** with KOTf are characterized by higher isotropization temperatures, and therefore provide a Φ_h mesophase with a higher thermal stability than the corresponding complexes with NaOTf.

The primary difference between the complexes of benzo-15-crown-5 with sodium and potassium salts consists in their stability constants and their stoichiometry. Benzo-15-crown-5 forms complexes in solution with both sodium and potassium cations [15, 16]. The stability constants of these complexes decrease with increasing cation size. In the solid state, benzo-15-crown-5 forms 1:1 complexes with sodium cations and 2:1 complexes with potassium salts [16]. No information is available for the stoichiometry of these complexes in the liquid crystalline phase. However, we can speculate that their behavior should follow the same general trend observed in the crystalline phase. Sodium prefers to be hexa-coordinated within the crown cavity, but benzo-15-crown-5 provides only five coordination sites. Therefore, the sixth coordination site is available for interaction with the counteranion or with a neighboring receptor. Potassium, which prefers to be hepta- or hexa-coordinated, is too large to fit within the crown ether cavity and is, therefore, complexed in a sandwich manner by 2 moles of benzo-15-crown-5. Consequently, less potassium salt is required to suppress the crystallization of **12-ABG-B15C5** and to generate a Φ_h mesophase.

Upon complexation of **12-ABG-B15C5** with more than 1.0 mole KOTf per mole **12-ABG-B15C5**, $T_{i-\Phi h}$ decreases slightly and then remains nearly constant (Fig. 4d). On the other hand, $T_{i-\Phi h}$ of the complexes of **12-ABG-B15C5** with more than 1.0 mole NaOTf per mole **12-ABG-B15C5** continues to increase up to a molar

ratio of 2.0. Transition temperatures of these complexes were not observed by DSC during the cooling scan at salt concentrations greater than 1.4 due to thermal decomposition of the sample during the first heating scan. However, characteristic fan-shaped textures were observed by thermal optical polarized microscopy prior to decomposition at NaOTf/**12-ABG-B15C5** molar ratios greater than 1.4. Since benzo-15-crown-5 forms 1:1 complexes with sodium cations, it is unexpected that more than a 1:1 molar ratio of NaOTf: crown ether in this system results in further stabilization of the mesophase. It is possible that the crown ether behaves both as a selective *endo*-receptor and as a nonselective solventlike *endo*-receptor in the liquid crystalline phase. Therefore, **12-ABG-B15C5** may dissolve larger amounts of salt than expected based on the behavior of benzo-15-crown-5 in solution and in crystalline phases.

The complex of **12-ABG-B15C5** with 0.6 mole NaOTf (**12-ABG-B15C5-0.6**) was characterized in the crystalline and Φ_h mesophase by SAXS and WAXS experiments. The poorly developed crystalline phase, which can be observed only during the first heating scan or after subsequent annealing, shows numerous weak reflections indicative of a lamellar crystalline structure. In the Φ_h mesophase, three reflections with d spacings in the ratio $d_{100}^{hex}:d_{110}^{hex}:d_{200}^{hex} = 1:1\sqrt{3}:1/2$, characteristic of the Φ_h mesophase, were observed. The radius of the cylindrical column ($R_{exp} = a/2$) and the side length of the hexagonal column ($S_{exp} = 2R/\sqrt{3}$) were determined from the hexagonal lattice parameter ($a = d_{100}^{hex}/\sqrt{3}$) to be 28.5 and 32.9 Å , respectively.

In order to derive conclusions about the molecular arrangement of **12-ABG-B15C5** within the self-assembled supramolecular columns, molecular models were constructed based on the conformation of related compounds as determined by crystallographic analyses [11]. A possible molecular arrangement is shown in Fig. 4(a) in which the crown ether moieties are arranged side by side within the center of the column layer. The aromatic moieties form a rigid inner core surrounding the melted crown ether *endo*-receptors. The melted alkyl tails of the *exo*-receptor radiate toward the column periphery and may fill the empty space within their own column or interdigitate into the empty space of adjacent columns. The experimentally determined density of the supramolecular structure obtained by complexation indicates that five or six tapered units reside within the column center. The crown ether *endo*-receptors may be stacked on top of each other, forming five or six continuous channel-like structures down the column axis. Ionic interactions between complexed and uncomplexed crown ether structural units provide the driving force for this layer–column transformation.

The structure of the taper-shaped structural unit, **12-ABG-15C5**, derived from the more conformationally flexible **15C5** *endo*-receptor unit, is shown in Fig. 5(a). The dependence of the transition temperatures of **12-ABG-15C5** and its complexes with NaOTf determined by DSC during the first cooling scan are plotted in Fig. 5(b). The dependence of the transition temperatures of **12-ABG-15C5** and its complexes with NaOTf determined by DSC during the first cooling scan are plotted in the same figure for comparison.

Compound **12-ABG-15C5** is also crystalline and melts into an isotropic liquid at 60°C. This melting temperature is 36°C lower than that observed for **12-ABG-B15C5**. Complexation with as little as 0.2 mole NaOTf per mole **12-ABG-15C5** results in the formation of a monotropic Φ_h mesophase. As the amount of NaOTf is increased to 0.5 mole, the Φ_h mesophase becomes enantiotropic. In the same manner
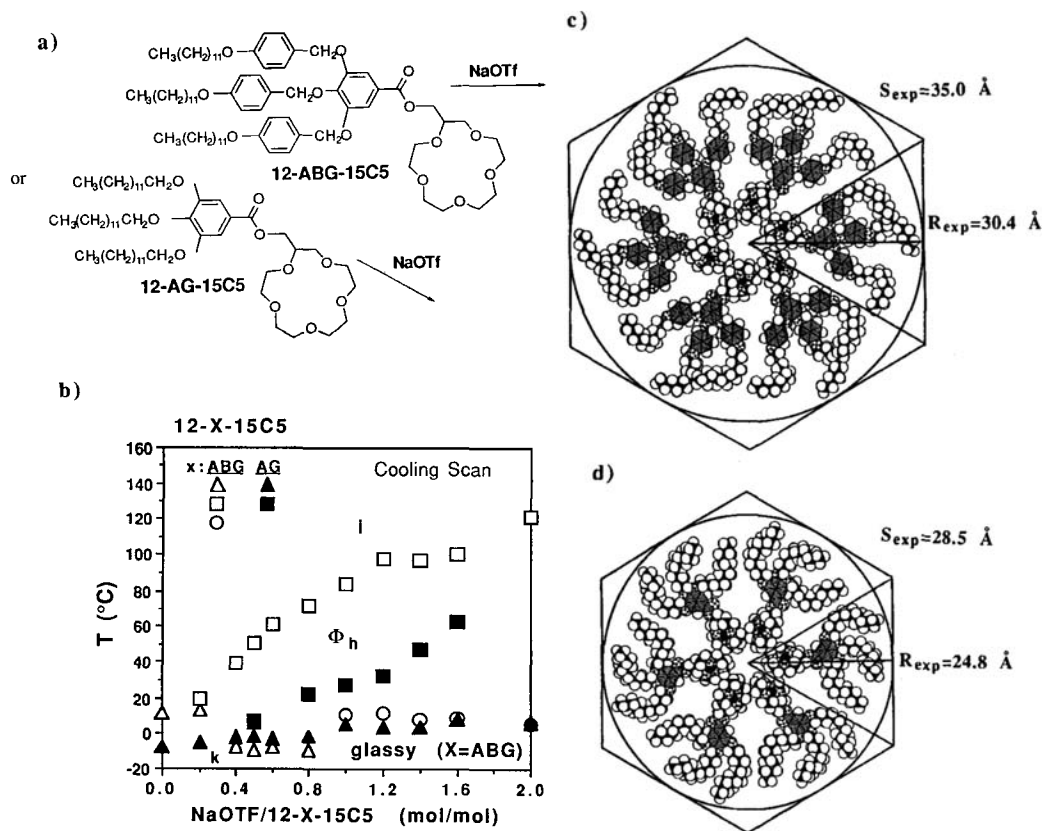
FIG. 5. Schematic representation of the complexation of **12-X-15C5** (X = ABG, AG) with sodium triflate (NaOTf) (a). The dependence of the phase transition temperatures of the complexes of **12-X-15C5** (X = ABG: (○) T_g; (△) T_{i-k}; (□) $T_{i-\Phi h}$; and X = AG: (▲) T_{i-k}; (■) $T_{i-\Phi h}$) (data from the first DSC cooling scan) (b). Schematic representation of a cross section of the supramolecular column formed upon complexation of **12-ABG-15C5** (c) and of **12-AG-15C5** (d) with NaOTf.

as **12-ABG-B15C5**, increasing the amount of NaOTf suppresses crystallization and increases $T_{i-\Phi h}$. A Φ_h mesophase was observed by optical polarized microscopy for complexes of **12-ABG-15C5** with as much as 2.0 moles NaOTf. Higher concentrations were not investigated. Compound **12-ABG-15C5** displayed a lower $T_{i-\Phi h}$ than **12-ABG-B15C5** over the entire composition range. This difference varied between 10 and 20°C.

The phase behavior of the complex of **12-ABG-15C5** with 1.6 moles NaOTf was characterized by SAXS and WAXS experiments. The crystalline phase displays numerous comparatively sharp reflections extending to wide angles. The first four reflections index on a hexagonal lattice. This is in contrast to the lamellar structure observed in the crystalline phase of complexes of **12-ABG-B15C5**. The observed hexagonal packing in **12-ABG-15C5** is most probably a consequence of the increased conformational flexibility of the **15C5** moiety. This flexibility results in

fewer conformational restrictions upon complexation and may lead to faster and eventually stronger complexation with alkali metal cations which in turn results in increased interactions between complexed and uncomplexed crown ether structural units within the column center. The role of preorganization of the conformationally flexible *endo*-receptor is a well-established event in molecular recognition processes [17].

In the Φ_h mesophase, **12-ABG-15C5** displays the three reflections characteristic of the Φ_h mesophase. An arrangement similar to that described for the Φ_h mesophase of **12-ABG-B15C5** is depicted in Fig. 5(c). R_{exp} and S_{exp} were determined to be 30.4 and 35.0 Å, respectively. For reasons that will be discussed later in this section, it is most probable that six molecules of **12-ABG-15C5** reside within the column center. This quantity is within the limits imposed by the experimentally determined density of the complex. In all other respects, the Φ_h mesophase of **12-ABG-15C5** is structurally similar to that described for **12-ABG-B15C5**.

Figure 5(a) shows the structure of **12-AG-15C5**. This tapered unit is structurally similar to **12-ABG-15C5**. However, the benzyl ether moieties are absent in the alkyl tails of the **12-AG-15C5** *exo*-receptor. The taper-shaped *exo*-receptors derived from *n*-alkyloxy tails are synthetically more accessible and thermochemically more stable than their *n*-alkyloxybenzyloxy counterparts. The dependence of the transition temperatures of **12-AG-15C5** and its complexes with NaOTf determined by DSC during the first cooling scans are plotted in Fig. 5(b).

Compound **12-AG-15C5** is crystalline and melts into an isotropic liquid at 32°C. The complexes of **12-AG-15C5** with NaOTf are crystalline over the entire composition range (0–2.0 mol/mol) but exhibit a monotropic Φ_h mesophase at NaOTf/**12-AG-15C5** molar ratios of 0.5 and greater. The $T_{i-\Phi h}$ is 50–60°C lower than the corresponding transitions in **12-ABG-15C5**. Furthermore, a T_g is not observed due to crystallization during the cooling scan. The kinetically controlled crystallization process is faster for the *exo*-receptor of **12-AG-15C5** than that of **12-ABG-15C5** due to the absence of the benzyl ether moieties.

The phase behavior of the complex of **12-AG-15C5** with 1.6 moles NaOTf was also characterized by WAXS and SAXS experiments. The crystalline phase is a double layer structure with the crown ethers arranged head-to-head within the layers. This is in contrast to the hexagonal order observed in the crystalline phase of **12-ABG-15C5**. In the Φ_h mesophase of **12-AG-15C5**, only two reflections were observed at low angles. The fact that the corresponding spacings are in a 2:1 ratio is indicative of a Φ_h mesophase. The R_{exp} and S_{exp} determined from the hexagonal lattice parameter are 24.8 and 28.5 Å, respectively. The smaller dimensions are expected as a result of the absence of the benzyl ether moieties. The structure of the Φ_h mesophase of **12-AG-15C5** is shown in Fig. 5(d). From these data it is obvious that the benzyl ether moieties stabilize the Φ_h mesophase of the taper-shaped structural unit by suppressing crystallization of the alkyl tails and increasing the width of the tapered *exo*-receptor at the column periphery.

Figure 6 shows a comparison of the idealized lowest energy conformation of the cross section of the Φ_h mesophase of **12-ABG-15C5** and the corresponding structure with melted alkyl tails. Similar depictions of **12-ABG-B15C5** and **12-AG-15C5** have been omitted for brevity. In the minimum energy conformation, the alkyl tails are fully extended in an all-*trans* configuration. The theoretical radius (R_{th}) for the minimum energy conformation was determined by measuring the dis-
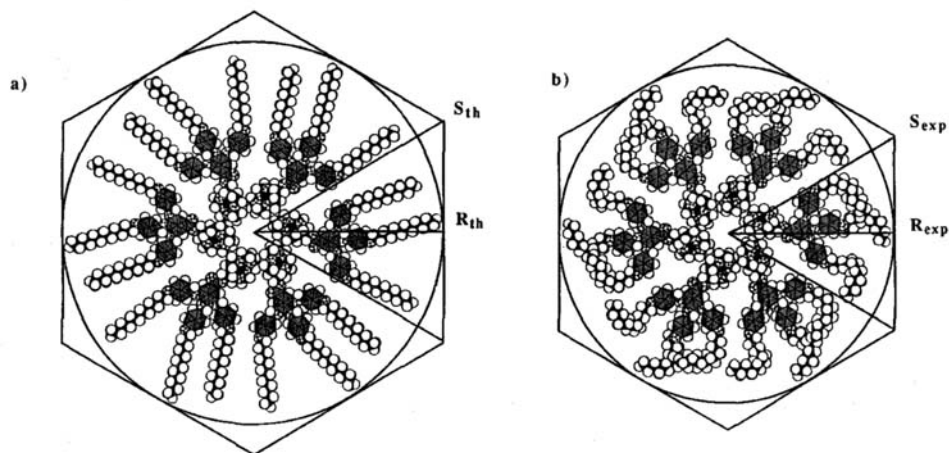
Compound	No. of Molecules	R_{th} (Å)	R_{exp} (Å)	S_{exp} (Å)	Shrinkage (%)
12-ABG-B15C5	5	40.8	28.5	32.9	67
12-ABG-15C5	6	41.2	30.4	35.0	57
12-AG-15C5	6	34.5	24.8	27.7	59

FIG. 6. Schematic representation of a cross section of the column generated by the complexation of **12-ABG-15C5** with 1.6 moles sodium triflate (NaOTf). (a) Top view containing six molecules of **12-ABG-15C5** with the alkyl tails extended. (b) Top view containing six molecules of **12-ABG-15C5** with the alkyl tails melted to match R_{exp}. Similar data for **12-ABG-B15C5** and **12-AG-15C5** are presented in the table.

tance from the center of the column to the outermost alkyl tail of the respective molecular models. In Fig. 6, R_{th} is compared to the experimental radius (R_{exp}) determined by x-ray scattering. In each case a larger value of R_{th} can be reconciled with the observed radius, R_{exp}, by shrinkage of the alkyl tails. This shrinkage should be confined to the alkyl tails due to the rigidity of the aromatic internal core of the assembly. The shrinkage is shown in Fig. 6 for the three supramolecular assemblies. From the shrinkage, a reasonable estimate of the number of molecules in a column cross-section can be determined. In the case of **12-ABG-B15C5**, six molecules would result in a larger internal core and a correspondingly larger alkyl tail shrinkage of 78%. Additional work in our laboratory has shown alkyl tail shrinkages of 50–60% [8–10]. Therefore, a model composed of five molecules of **12-ABG-15C5** seems more reasonable. In the case of **12-ABG-15C5**, models composed of five and six molecules give acceptable shrinkages of 51 and 57%, respectively. The R_{exp} of the cross section of the self-assembled supramolecule derived from **12-ABG-15C5** is ~2 Å larger than the corresponding radius of that derived from **12-ABG-B15C5**. However, the end-to-end distance of the minimum energy conformation of an isolated molecule of **12-ABG-15C5** is ~3 Å shorter than the corresponding dimension of **12-ABG-B15C5**. However, when the supramolecular cylinder of **12-ABG-15C5** is composed of six taper units per column layer instead of five, it would be expected to exhibit a larger R_{exp}, as is indeed the case.

Oligooxyethylenic Segments as *Endo*-Receptors: A Comparison between Supramolecular and Molecular "Polymer Backbones"

12-ABG-nEO-OH and **12-ABG-nEO-PMA**, shown in Fig. 7, self-assemble similarly with the systems based on crown ethers as *endo*-receptor. In this case the cation selective crown ether *endo*-receptor of the tapered subunit from the previous molecules was replaced with the nonselective oligooxyethylenic *endo*-receptor. **12-ABG-nEO-OH** are analogous to **12-ABG-15C5** shown in Fig. 4. The value of n indicates the number of oligooxyethylene segments and varies from $n = 1$ to 4. **12-ABG-nEO-PMA** are the polymeric analogs of **12-AGB-nEO-OH**. All compounds form an enantiotropic Φ_h mesophase which was characterized by a combination of x-ray scattering, thermal optical polarized microscopy, and DSC experiments [18]. The mechanism of formation and stabilization of the self-assembled supramolecular columns is similar for both **12-ABG-nEO-OH** and **12-ABG-nEO-PMA** but provides access to a systematic investigation of the difference between the two systems as n is varied.

As n is increased from 1 to 4 the Φ_{h-i} transition temperatures (T_i) for both systems decrease at a similar slope. For all n presented here, T_i of **12-ABG-nEO-PMA** is consistently about 45°C higher than that of the low molar mass compounds **12-ABG-nEO-OH** (Fig. 7a). Figure 7(b) shows the dependence of the experimentally determined column radius (R_{exp}) as a function of n. Increasing n causes R_{exp} to increase. The column radii of the polymers are 2 to 4 Å larger than their corresponding monomer compounds **12-ABG-nEO-OH**.

Molecular models were constructed for all compounds to provide explanations for these observations in phase behavior and column diameter [18, 19]. Figure 7(c) illustrates a model of a cross section of the cylinder formed by **12-ABG-nEO-OH** with the alkyl tails and the flexible oligooxyethylene spacer melted so that the radius of the model is equivalent to the value determined by x-ray scattering experiments. The oligooxyethylene spacer is confined to the core of the supramolecule as a result of the tapered shape, packing efficiency, and other factors. A more detailed discussion of this system will be presented in the following paragraph and in Fig. 9. Figure 7(d) shows a cross section of the cylinder formed by **12-ABG-nEO-PMA**. The flexible oligooxyethylene spacer in the core of both compounds complexes alkali metal salts. The phase behavior of both systems was characterized as a function of the amount of LiOTf in the complex. Some of these results will be presented in Fig. 8. As a result of these experiments, Li cations (represented as filled atoms) are placed in the most likely sites of coordination within the cross section of the models in Figs. 7(c) and 7(d).

The model of **12-ABG-nEO-OH** in Fig. 7(c) demonstrates that the formation of the supramolecular column results from several factors. The tapered and effectively flat shape favors packing into a cylindrical arrangement as opposed to lamellar or spherical packing. As a result of the molecular design, the polar ω-hydroxyoligooxyethylene segments are concentrated in the core of the assembly. The main forces responsible for this arrangement are hydrogen bonding (H-bonding) and electrostatic attractive interactions of the flexible oligooxyethylene segments as well as microsegregation of these polar groups from the nonpolar aliphatic and aromatic groups at the column periphery. When LiOTf is added, the microsegregation and attractive interactions in the core of this assembly are enhanced by the complexation
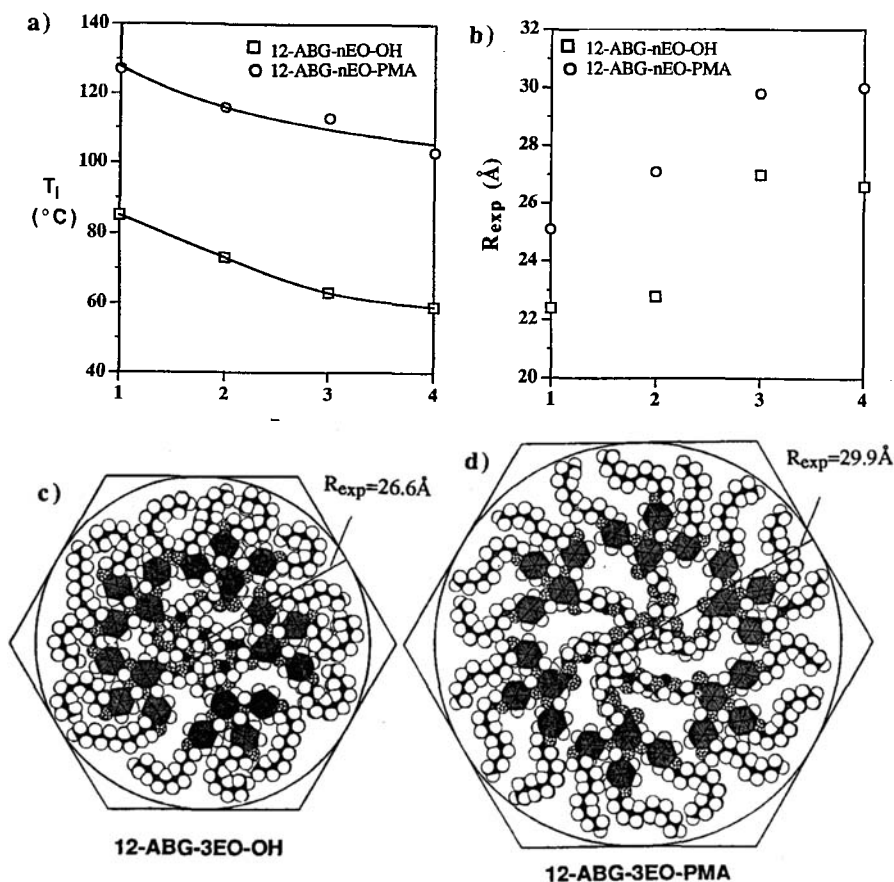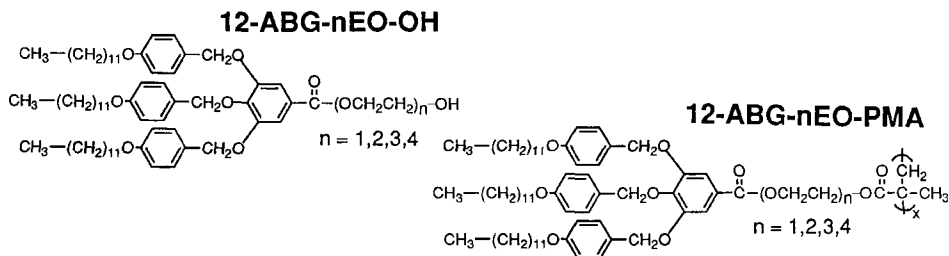
FIG. 7. The dependence of T_i of **12-ABG-nEO-OH** (□) and **12-ABG-nEO-PMA** (○) versus n (data from the first DSC heating scans) (a). The dependence of R_{exp} of **12-ABG-nEO-OH** (□) and of **12-ABG-nEO-PMA** (○) versus n (b). A model of the cross section of the column formed by **12-ABG-3EO-OH** (c). A model of the cross section of the column formed by **12-ABG-3EO-PMA** (d).

of the salt which provides a thermodynamic stabilization to the self-assembled structure and shifts the T_i to higher temperatures. The effect of the contribution of the polymer backbone is illustrated with the model in Fig. 7(d). The linear nature of the polymer backbone imposes restrictions on the placement of the taper-shaped side groups within the column that are not present with the low molar mass analogs **12-ABG-nEO-OH**. Based on x-ray scattering, density (obtained at 23°C), and an assumed layer thickness of the cross section (based on a literature value), an approximate of 6 tapered side groups must occupy a cross section of the column. It is assumed that the column is formed by a single polymer chain. There is not yet any definitive evidence to disprove this assumption. For the necessary amount of side groups to occupy a cross section of the column, the polymer backbone must adjust its conformation cooperatively.

The self-assembly of **12-ABG-nEO-PMA** can be qualitatively compared with **12-ABG-nEO-OH** with respect to the forces responsible for the self-assembly process. The replacement of the weak H-bonding of the pendant OH groups with the much stronger covalent bond to the polymer backbone provides a greater force holding the taper-shaped groups together and increases the thermodynamic stability of the supramolecular structure (see Fig. 7a). The disadvantage provided by the covalent attachment to the polymer backbone and the elimination of the pendant OH group is that the nonselective and flexible oligooxyethylene segments are not able to complex as much LiOTf or interact with the salt as efficiently in as in the low molar mass compounds **12-AGB-nEO-OH**.

The effect of the LiOTf on the phase behavior of the resulting complex is shown in Fig. 8 for the compounds **12-ABG-nEO-OH** [18, 19] with $n = 1$ to 4 and for the model compound **12-ABG-3EO-OCH₃** [18]. Figure 8(a) displays representative DSC traces of **12-ABG-3EO-OH** with increasing amounts of LiOTf. The peak associated with the T_i systematically increases as the amount of LiOTf increases, while the crystalline melting transition (k) remains constant. The effect of replacing the OH with a CH₃ group is shown in Fig. 8(b). The OH group provides stabilization to the self-assembled structure via H-bonding. The pendant OCH₃ group can only participate in weak electrostatic attractive interactions and introduces the possibility of repulsive steric interactions in the core of the supramolecular structure as a result of its increased size. Compound **12-ABG-3EO-OCH₃**, which contains an OCH₃ terminal group in the *endo*-receptor, exhibits a T_i about 40°C lower than **12-ABG-3EO-OH**, which has an OH terminal group in the *endo*-receptor. Also, **12-ABG-3EO-OCH₃** is not able to complex as much LiOTf as **12-ABG-3EO-OH**. The last value presented in Fig. 8(b) is 0.8 mole LiOTf per repeat unit. Above this value a crystalline phase appears which may be the result of the formation of LiOTf aggregates. It should be pointed out that amounts of LiOTf larger than 0.8 mole per mole **12-ABG-3EO-OH** and temperatures higher than 120°C cause Lewis-acid-catalyzed decomposition of the *p*-alkoxybenzyl ether groups. This produces the downward curvature of the T_i temperatures on cooling and second heating scans with increasing amounts of LiOTf (Fig. 8b).

The dependence of the transition temperature on the length of the oligooxyethylene spacer of **12-ABG-nEO-OH** plotted versus the amount of complexed LiOTf is shown in Fig. 8(c). **12-ABG-1EO-OH** and **12-ABG-2EO-OH** have short oligooxyethylene spacers and are able to complex 0.3 and 0.4 mole LiOTf per taper-shaped group, respectively. **12-ABG-3EO-OH** and **12-ABG-4EO-OH** have
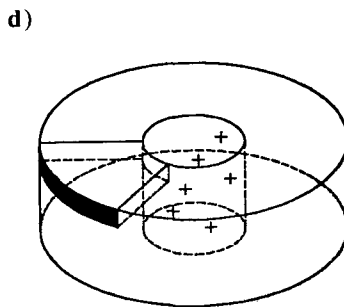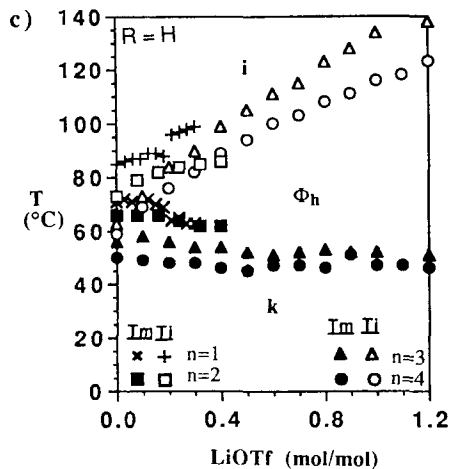
$CH_3-(CH_2)_{11}O$—⟨⟩—CH_2O

$CH_3-(CH_2)_{11}O$—⟨⟩—CH_2O—⟨⟩—$\overset{O}{\overset{\|}{C}}$—$(OCH_2CH_2)_n$—OR + LiOTf

$CH_3-(CH_2)_{11}O$—⟨⟩—CH_2O

R = H, CH_3
n = 1,2,3,4   **12-ABG-nEO-OR**

a)

b)

c)

d)
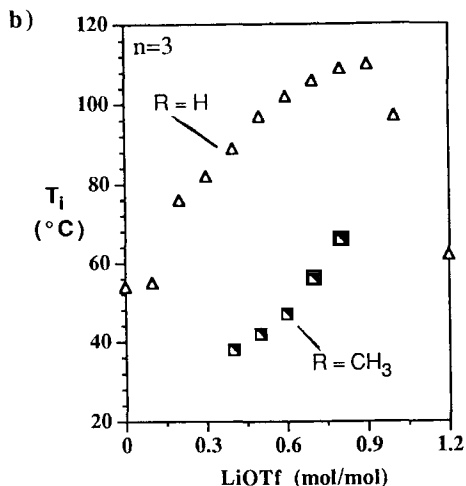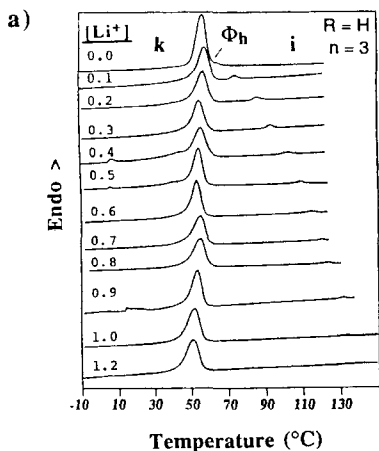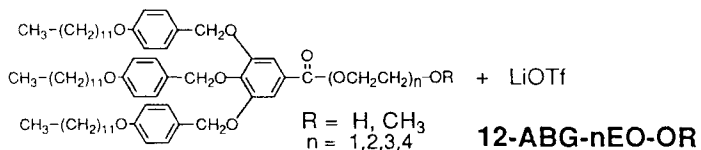
FIG. 8. (a) Representative DSC traces of **12-ABG-3EO-OH** with increasing concentrations of lithium triflate (LiOTf) per mole of **12-ABG-3EO-OH** ([Li$^+$]) (first DSC heating scans). (b) The dependence of the T_i for **12-ABG-3EO-OH** (△) and **12-ABG-3EO-OCH$_3$** (□) versus LiOTf concentration (data from the first DSC cooling scans). (c) The dependence of the T_m and T_i versus LiOTf concentration of **12-ABG-nEO-OH** for $n = 1$ (×, +), $n = 2$ (■, □), $n = 3$ (▲, △), and $n = 4$ (●, ○) (data from the first DSC heating scans). (d) A representation of the self-assembled cylindrical structure with dissolved salts in the core.

longer oligooxyethylene segments with a larger number of electron-rich donor oxygen atoms and are able to complex up to 1.2 moles LiOTf per taper-shaped group. Above this value, T_i values are in the range where decomposition begins to occur. This prevents determination of the upper limit of LiOTf that can be complexed.

It is now possible to make a quantitative comparison of the electrostatic, ionic, and H-bonding (i.e., supramolecular interactions) with molecular "interactions" (generated via a conventional molecular polymer backbone) responsible for generating this supramolecular architecture. It requires interactions in the core provided by 0.7 mole LiOTf per structural unit for the cylindrically-shaped structure formed by **12-ABG-3EO-OCH$_3$** to have the same thermodynamic stability that results from the H-bonding of the OH group of **12-ABG-3EO-OH** without complexed LiOTf (see Fig. 8b).

This provides a measure of the contribution of H-bonding to the self-assembly of the supramolecular cylinders. A direct comparison of the effect of a noncovalent (supramolecular) polymer backbone and a covalent (molecular) polymer backbone can be made by comparing **12-AGB-3EO-OH** and **12-ABG-3EO-PMA**. **12-ABG-3EO-OH** requires 0.65 mole LiOTf per structural unit in conjunction with the H-bonding present to equal the same thermodynamic stability of the cylinder that is generated by the polymethacrylate backbone (i.e., 45°C higher T_i, see Figs. 7a and 8c). In addition to providing a direct comparison between *molecular* and *supramolecular "polymer effects,"* these observations further highlight the structural tools that can be used to regulate the internal interactions of these tubular structures.

A representation of the self-assembled cylindrical supramolecular structure formed by these compounds is shown in Fig. 8(d) [19]. Cations (represented as the +'s) are placed in the core of this cylinder where the flexible oligooxyethylene segments reside. Questions remain about the location of the anions or about the possibility that the alkyl-phenyl and benzyl-phenyl ether oxygen atoms contribute to the complexation of high amounts of Li cations.

The main forces responsible for the self-assembly process that have been presented so far are dramatically illustrated with **m+1-AG-3EO-OH** and **12-AG-nEO-PMA** shown in Fig. 9 [20]. These compounds are of similar design to **12-ABG-nEO-OH** and **12-ABG-nEO-PMA** which are shown in Fig. 7, with the exception that the three benzyl ether groups from the *exo*-receptor are absent. This change decreases T_i approximately 50–70°C for most of the compounds and allows demonstration of the critical *exo*-molecular recognition interactions present in these systems. **12-AG-octyl-PMA** [20] is a model compound for **12-AG-3EO-PMA** and has an octyl spacer connecting the tapered side-group to the polymethacrylate backbone. Replacement of the triethyleneoxide spacer with an *n*-octyl spacer having the same number of atoms removes the electrostatic attractive interactions present in the core resulting from EO spacer, provides a slight increase in the rigidity of the spacer, and as a result of its hydrophobic character reduces the stabilization provided to the assembly via microsegregation of hydrophilic and hydrophobic functionalities. The DSC traces of **12-AG-nEO-PMA** with $n = 1$ to 4 and of **12-AG-octyl-PMA** are shown in Fig. 9(a). All **12-AG-nEO-PMA** display an enantiotropic Φ_h mesophase with T_i values between 51 and 54°C, as well as a crystalline (k) melting transition. **12-AG-octyl-PMA** is only liquid within the temperature range examined. The changes that result from replacing the EO spacer with a paraffinic spacer destroy its ability to form both k and Φ_h phases.
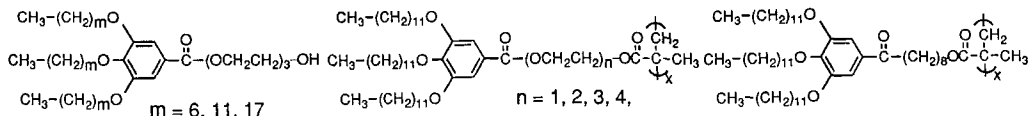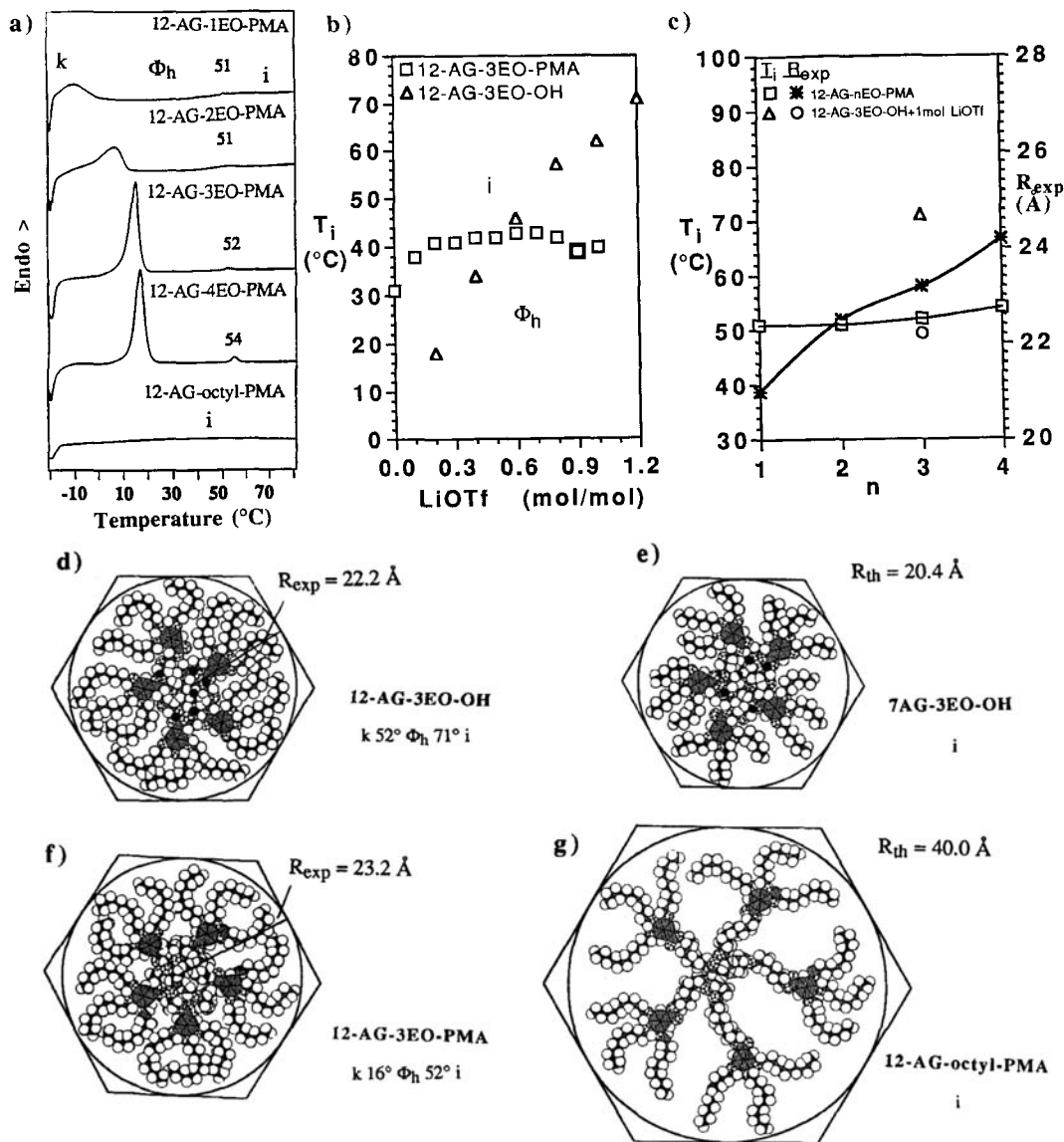
FIG. 9. (a) Representative DSC traces of **12-AG-nEO-PMA** for n = 1 to 4 and of **12-AG-octyl-PMA** (first DSC heating scans). (b) The dependence of the T_i for **12-AG-3EO-PMA** (□) and **12-AG-3EO-OH** (△) versus lithium triflate (LiOTf) concentration (data from the first DSC cooling scans). (c) The dependence of the T_i versus n (data from the first DSC heating scans) on the left y-axis and the dependence of the column radius determined from x-ray scattering experiments on the right y-axis for **12-AG-nEO-PMA** (□, ∗) and **12-AG-3EO-OH** with 1.0 mole of complexed LiOTf (△, ○). Molecular model cross sections of the cylindrically-shaped structures of: (d) **12-AG-3EO-OH**; (e) **7-AG-3EO-OH**; (f) **12-AG-3EO-PMA**; (g) **12-AG-octyl-PMA**.

A direct comparison of the self-assembly of the low molar mass **12-AG-3EO-OH** by only noncovalent interactions and the self-assembly that occurs as a result of covalent attachment to a polymethacrylate backbone in conjunction with noncovalent interactions (**12-AG-3EO-PMA**) is outlined in Fig. 9(b). T_i is plotted versus the amount of LiOTf present in the complex. Initially, the polymer backbone provides a greater thermodynamic stability to the self-assembled structure. At a LiOTf molar ratio of 0.6, the polymer and the low molar mass compounds have approximately equivalent T_i values. As the amount of LiOTf is further increased, the T_i of **12-AG-3EO-OH** continues to increase whereas the T_i of **12-AG-3EO-PMA** does not. The noncovalently bound **12-AG-3EO-OH** is able to adjust its position and conformation within the column to take advantage of enhanced interactions in the core that result from the complexed salt. Although the polymer backbone initially provides a greater thermodynamic stability to the supramolecular architecture by causing positional restrictions, at higher salt ratios these positional restrictions hinder the tapered side-groups from benefiting from the interaction resulting from the complexed LiOTf.

Molecular models of some of these compounds are presented in Figs. 9(d)–9(g). **12-AG-3EO-OH** is shown in Fig. 9(d). It forms a Φ_h mesophase upon the addition of LiOTf. **7-AG-3EO-OH**, which has shortened alkyl tails, is outlined in Fig. 9(e). The latter does not form a Φ_h mesophase upon the complexation of LiOTf. It can be observed from the models in Figs. 9(d) and 9(e) that the short alkyl tails of **7-AG-3EO-OH** are not sufficiently efficient to provide a hydrophobic barrier around the polar ω-hydroxyoligooxyethylene segments. A model of **18-AG-3EO-OH**, which has alkyl tails six methylenic units longer than **12-AG-3EO-OH**, is not shown in Fig. 9. It also forms a Φ_h mesophase, but has higher T_i than **12-AG-3EO-OH** at the same ratios of LiOTf [20]. The increase in T_i for **18-AG-3EO-OH** is attributed to the longer alkyl tails which provide a greater hydrophobic contribution to the microsegregation and thus stabilizes the cylindrically-shaped assembly. Models of **12-AG-3EO-PMA** and **12-AG-octyl-PMA** are shown in Figs. 9(f) and 9(g), respectively. The electrostatic attractive interactions that result from the oligooxyethylene spacer in **12-AG-3EO-PMA** (Fig. 9f) are absent in the paraffinic spacer of **12-AG-octyl-PMA** (Fig. 9g) and cannot hold the tapered side-groups in a close arrangement around the polymer backbone.

Compounds **m+1-AG-nEO-OH** and **12-AG-nEO-PMA** represent a self-assembled supramolecular system in which the molecular recognition interactions are delicately balanced. Structural changes which affect these interactions produce dramatic changes in the diameter and flexibility of the self-assembled cylinders, and subsequently in the thermodynamic stability of the Φ_h mesophase resulting from them.

Endo-Receptors Based on H-Bonding

Compounds **n+1-AG-DA2**, which are shown on the top of Fig. 10, form cylindrically-shaped supramolecules by somewhat different interactions and molecular packing principles than the previous systems presented in this paper.

n+1-AG-DA2 have two taper groups connected at the 1 and 2 positions of an ethylenic spacer by benzamido functionalities. They form a Φ_h mesophase, depending on the tail length, as a result of H-bonding [21]. **n+1-AG-DA2** can form these

$CH_3-(CH_2)_nO$

$n = 0,1,3,4,5,6,9,10,11,13,15,17$

n+1-AG-DA2

$n = 11$
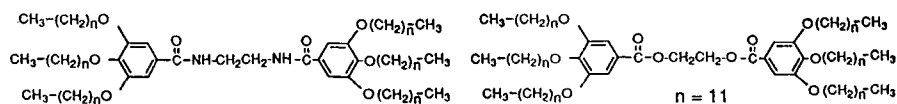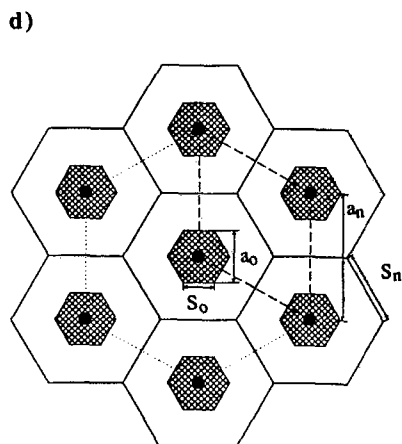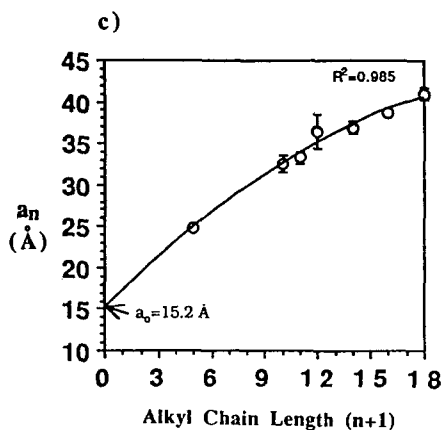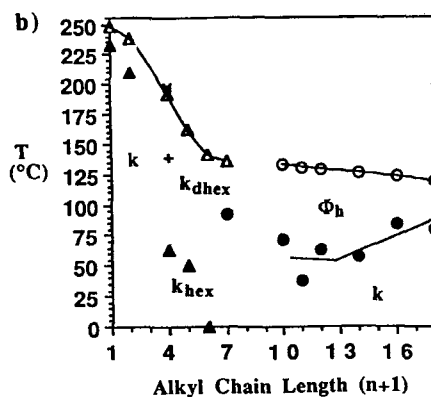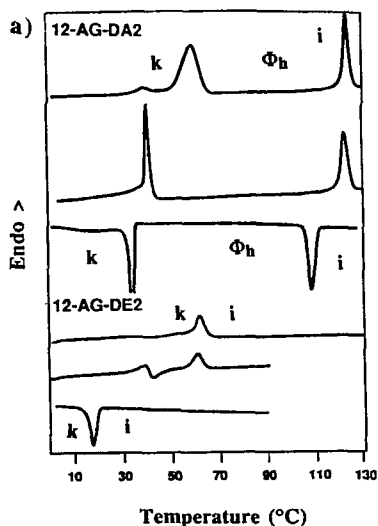
12-AG-DE2

FIG. 10. (a) DSC traces from the first heating scan, second heating scan, and first cooling scan (top to bottom) for **12-AG-DA2** and **12-AG-DE2**. (b) The phase behavior of n +1-AG-DA2 versus alkyl tail length ($n + 1$). (c) Extrapolation of the experimentally measured column radius (a_n) determined from x-ray scattering experiments in the k_{hex} of Φ_h phases versus alkyl tail length. (d) Illustrative definitions of a_n, a_0, S_n, and S_0 for the hexagonal columnar phase.

H-bonds between the NH hydrogen donor (H-donor) and C=O hydrogen acceptor (H-acceptor) groups. A more detailed discussion of a possible H-bonding motif within the columns will be presented in Fig. 11. **12-AG-DE2** was synthesized as a model compound for **12-AG-DA2** since it has the same molecular structure with the exception that the NH groups have been replaced with an ester O atom. For **12-AG-DE2** the C=O groups are capable of forming H-bonds with a H-donor group. The replacement of the NH group by an O eliminates the H-donor group from the molecule. Consequently, **12-AG-DA2** (also all **n+1-AG-DA2**) in the bulk form can form H-bonds whereas **12-AG-DE2** cannot, unless a second component bearing a H-donor group is added. DSC scans of pure **12-AG-DA2** and **12-AG-DE2** are shown in Fig. 10(a). Both compounds have similar structures so it is not surprising that they exhibit identical melting temperatures on the first DSC heating scan (T_m = 63°C). As a result of **12-AG-DA2**'s functional capability to self-H-bond in bulk form, it maintains a Φ_h mesophase up to 129°C. **12-AG-DE2**, which cannot self-H-bond, melts from a crystalline phase (k) directly into an isotropic liquid (i). The self-H-bonding is one of the essential factors required by these molecules to form a cylindrically-shaped assembly which generates a Φ_h mesophase.

Another critical factor is the length of the alkyl tails. Figure 10(b) shows the phase behavior of **n+1-AG-DA2** determined by x-ray scattering, thermal optical polarized microscopy, and DSC experiments as a function of the alkyl tail length ($n + 1$) [21]. **n+1-AG-DA2** with alkyl tail lengths ≥ 10 methylenic units display a Φ_h mesophase. When the alkyl tail length is ≤ 7 methylenic units, these compounds exhibit only crystalline phases. For **n+1-AG-DA2** with $n = 3, 4, 5$, and 6, the uppermost phase is identified as a distorted crystalline hexagonal phase (k_{dhex}). **5-AG-DA2** displays a truly hexagonal crystalline phase (k_{hex}) at room temperature. In Fig. 10(c), extrapolation of the experimentally determined column diameters (a_n) in the Φ_h and k_{hex} phases to an alkyl chain length of 0 methylenes gives a rigid core diameter (a_0) of 15.2 Å (refer to Fig. 10d for illustrative definitions of a_n and a_0). This value is used to construct molecular models as an approximate of the core diameter.

Based on these experimental results, we have been able to construct an estimated model of the molecular packing and H-bonding contacts within the column. In formulating this model we have taken into account the experimentally determined column diameters, the extrapolated core diameter, a representative density measurement for **12-AG-DA2** (obtained at 23°C), optimum H-bonding distances and angles for amides, additional attractive and repulsive van der Waals interactions, and the possibility of intramolecular H-bonds versus intermolecular H-bonds. Also, the packing of related bisamides shown in Fig. 11(a) obtained from their crystal structure was taken into consideration. The most likely model of the column core which can explain all results is shown in Fig. 10(b). This is a side view of the column formed by **n+1-AG-DA2** with $n ≥ 9$. H-bonding occurs intermolecularly vertically along the column axis. The ethyl spacer is in a low energy *trans* conformation. The aromatic rings are shown relatively perpendicular to the column axis. It is possible that they are tilted or oscillate when in the Φ_h phase. This H-bonding motif results in a net translation which would produce a tilted column. To offset this we have tilted the molecules along the column axis.

Figure 11(c) shows the top view of a cross section of the column formed by this packing. The alkyl tails have been added and melted above and below the plane

a)

R=H, CH3

b)

c)

$R_{exp} = 20.5$ Å

$<a_0> = 16.6$ Å

d)
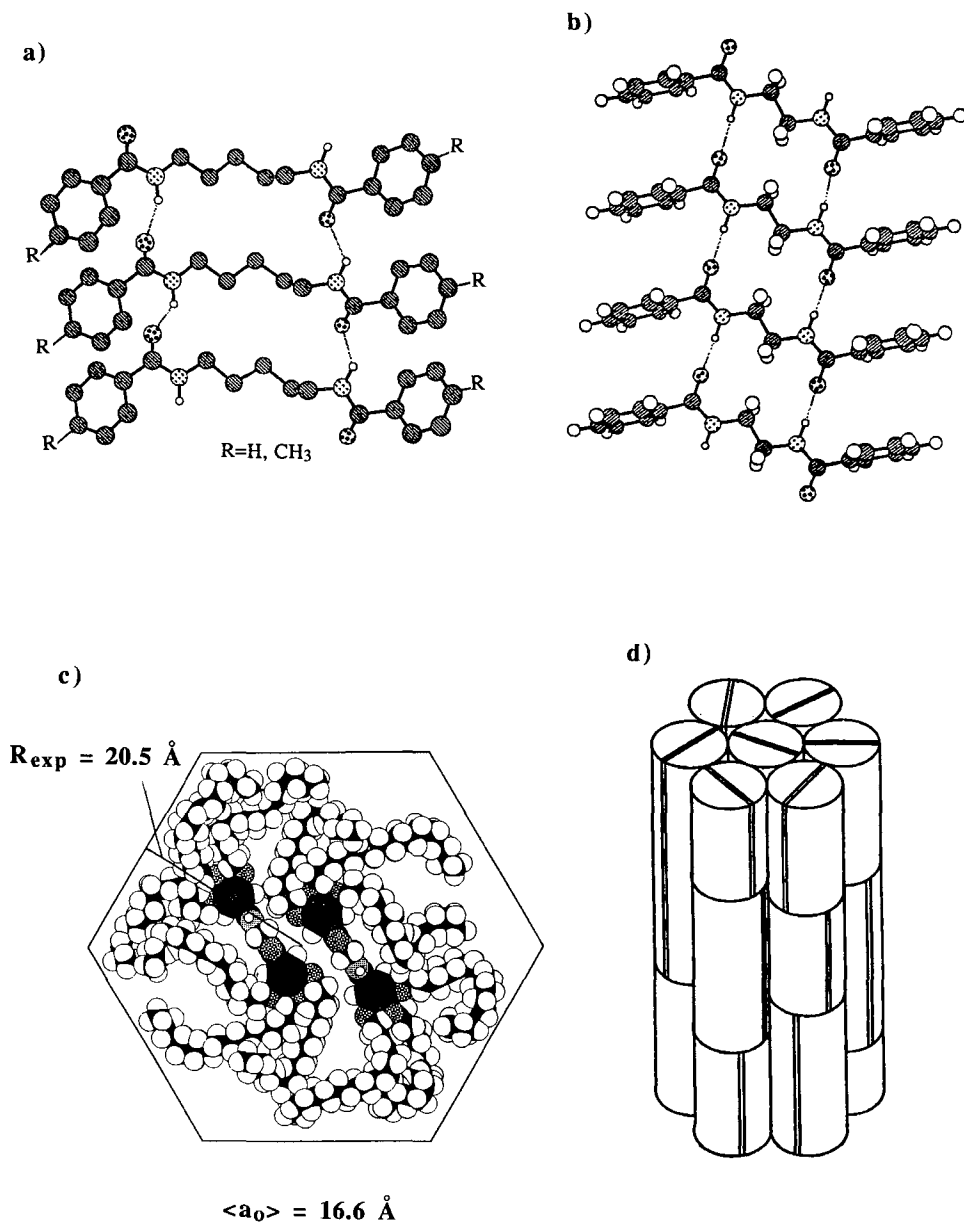
FIG. 11.   (a) Pleated ribbon packing of molecules of related bisamides in the crystal structure. (b) A side view of the proposed H-bonding in the Φ_h mesophase of **n+1-AG-DA2** (for $n + 1 \geq 10$) along the column axis. (c) A top view of a cross section of the column formed by **18-AG-DA2** with alkyl tails melted. (d) A representation of 2 columns (semicolumns) of **n+1-AG-DA2** forming a column which packs into the hexagonal lattice of the Φ_h mesophase.

of the cross section. Apparent areas of void would be filled by the melted alkyl tails from cross sections above and below this cross section. In order to meet the requirements of the results obtained from x-ray scattering and density measurements, the column must be composed of two independent (semicolumns) which are H-bonded along the column axis and pressed against each other in the middle. Although there may exist some attractive or repulsive interactions at the interface between the two semicolumns (see the apparent lock-and-key generated at the interface), the principal forces that lead to this type of packing arrangement would be the tetra coordinate H-bonding of the molecules along the column axis and the packing efficiency of the melted alkyl tails surrounding the rigid aromatic cores.

Careful observation of the aromatic core of this model reveals that it has an elliptical shape rather than a circular one. This provides a possible explanation for the phase behavior presented in Fig. 10(b). With long alkyl tails ($n + 1 \geq 10$) the melted alkyl periphery may average to a circular shape within a cross section of the column, thereby producing a symmetrical cylinder. But for shorter alkyl tails ($n + 1 \leq 7$), this averaging may not be able to produce a circular-shaped periphery as a result of the molecular placement in the core. Without a circular shape, the columns cannot pack into a regular hexagonal lattice. The net result would be a distorted hexagonal lattice, and indeed a distorted hexagonal phase (k_{dhex}) is observed. Lack of sufficient melted alkyl content can explain the change from a liquid crystalline phase to a crystalline phase that occurs with this decrease in alkyl tail length. A minimum amount of disordered alkyl chains between the columns is needed to disrupt the registry of the layers between the columns and produce a liquid crystalline phase as opposed to a crystalline phase. Decreasing the alkyl tails from ten to seven methylenic units falls below this minimum amount.

Figures 11(d) and 12 illustrate the proposed different mechanisms of the self-assembly of cylindrically-shaped tubular supramolecular architectures presented in this paper [18, 20, 22]. Figure 11(d) illustrates the semicolumns of **n+1-AG-DA2** which form cylinders that pack into a hexagonal lattice generating a Φ_h mesophase. Figure 12 shows different representations of what the spontaneous packing of the side groups might possibly be for the polymers (and monomers) which form the tubular supramolecular architectures presented here. Possibly they may pack tightly or loosely to form disklike substructures which pack into a column. Or there may be a kind of helical packing that results from the linear nature of the polymer backbone. Additionally, there is also the possibility that two or more polymer chains cooperatively form a column.

The different approaches used to generate tubular supramolecular architectures are summarized in Fig. 13. With these structural and functional changes, the T_i of these Φ_h phases generated from the supramolecular cylinders have been controlled within the temperature range of 7 to 148°C, while the measured column diameters varied in the range of 42 to 61 Å, as expected, based on the dimensions of the individual molecular subunits. As presented in detail elsewhere [22], the taper-shaped subunits bearing different *endo*-receptors can co-assemble cooperatively to form similar structures subject to the limitations resulting from spatial packing as well as the thermodynamic and kinetic factors of the recognition processes. For example, the tapered groups with different lengths of the ω-hydroxyoligooxyethylene groups co-assemble over the entire range of compositions. However, the tapered groups with similar lengths of the oligooxyethylenic *endo*-receptor but terminated
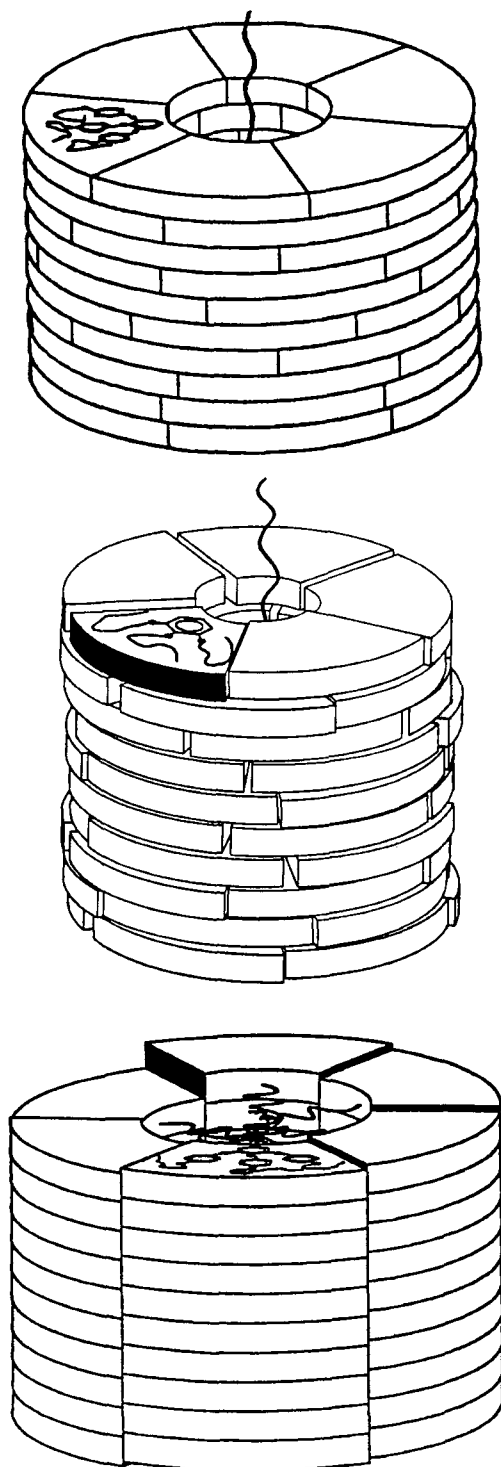
FIG. 12.   Different possibilities of the packing of the tapered side groups of the polymers that form tubular supramolecular architectures.

$-\text{ER}_1$

$+$

$-\text{ER}_2$

$\underline{\text{ER}_1 \text{ or } \text{ER}_2}$

$$-(OCH_2CH_2)_n-O\overset{O}{\underset{\parallel}{C}}-\overset{CH_2}{\underset{x}{C}}-CH_3$$

$-(OCH_2CH_2)_n-OH$

$-NHCH_2CH_2NH-$
$-CE$
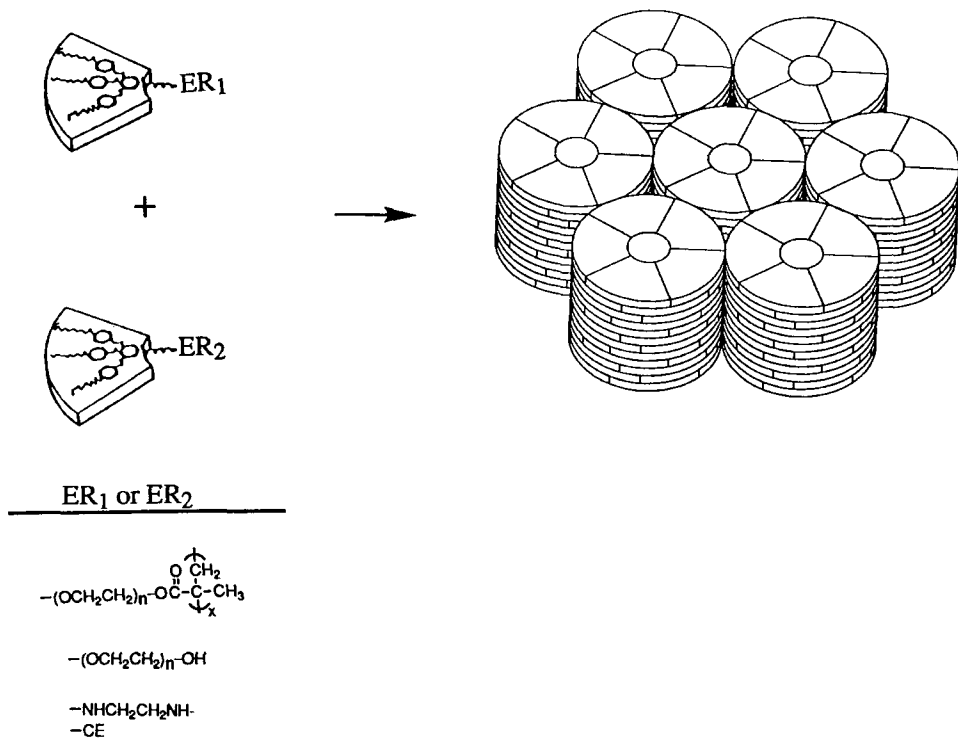
FIG. 13.   Summary of the different *endo*-receptors used to generate tubular supramolecular assemblies and the co-assembly of the taper-shaped groups that have different *endo*-receptors into a single cyclinder.

FIG. 14.   The theoretical and experimental dependence of the isotropization temperature (T_i) of cyclic and linear main-chain liquid crystalline polymers on their degree of polymerization (DP). Both T_i and DP are in arbitrary units.

FIG. 15. Conformational isomerism of TPB and its cyclization with 1,10-dibromodecane under high-dilution conditions.
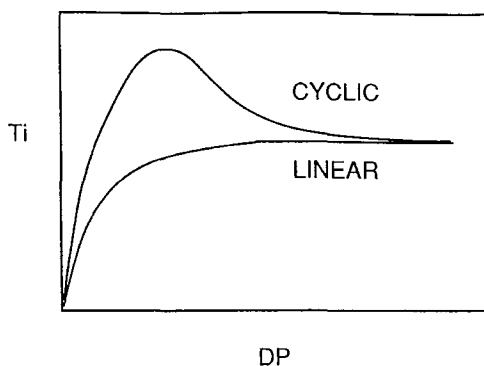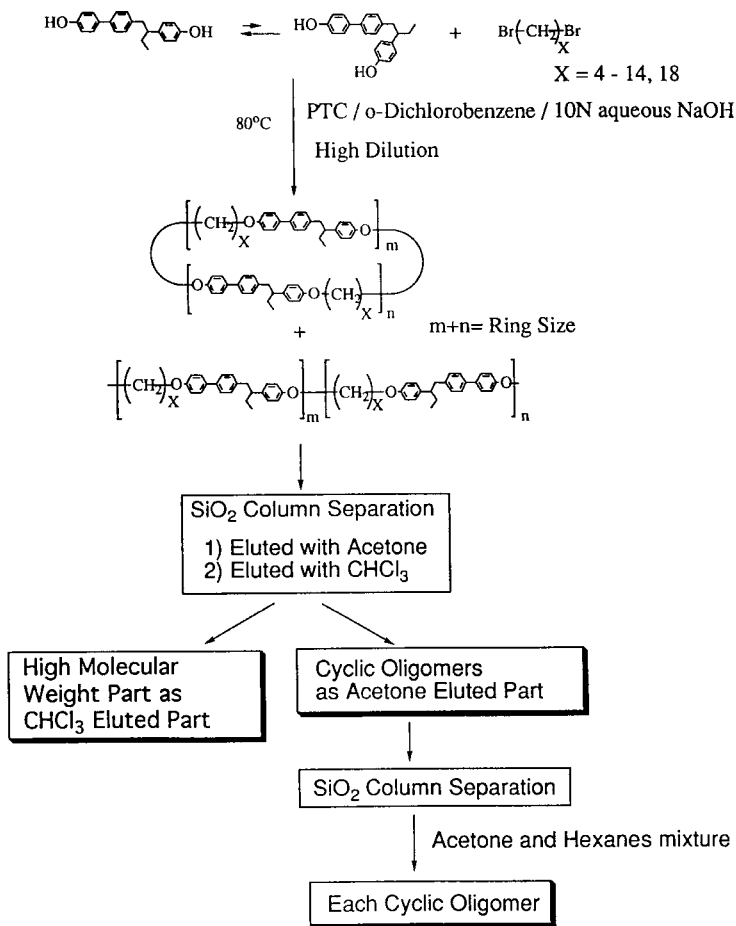
by a pendant OH and a covalent polymer backbone co-assemble only within a limited range of composition. This co-assembly process is considerably enhanced via complexation with alkali-metal salts. On the other hand, the tapered groups with ω-hydroxyoligooxyethylene and crown ether *endo*-receptors do not co-assemble in the presence of NaOTf but rather self-assemble into independent columns composed of only one kind of tapered subunit as a result of their considerably different strengths and rates of self-assembly versus co-assembly via complexation with salts.

The supramolecular cylindrical architectures outlined in Fig. 13 provide an entry into the molecular recognition directed self-assembly via principles which resemble those of the self-assembly of TMV. So far we can tailor-make the external diameter of these cylinders only within a very limited range. The same can be stated about the diameter of the channel penetrating through these architectures. These supramolecular cylinders self-assemble not only in the melt phase but also in solution. The surface of these cylinders can be tailor-made by chemical modification reactions performed on the outer edge of the *exo*-receptors. This work is only at the
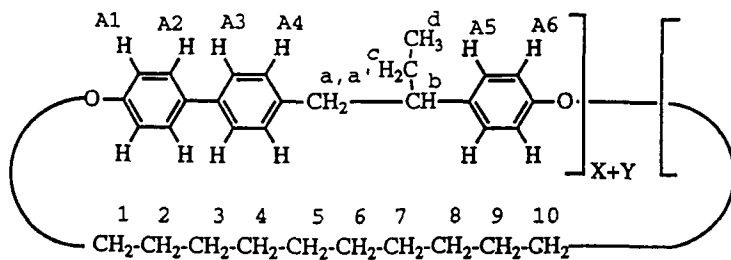
X+Y= Ring Size

Ring Size
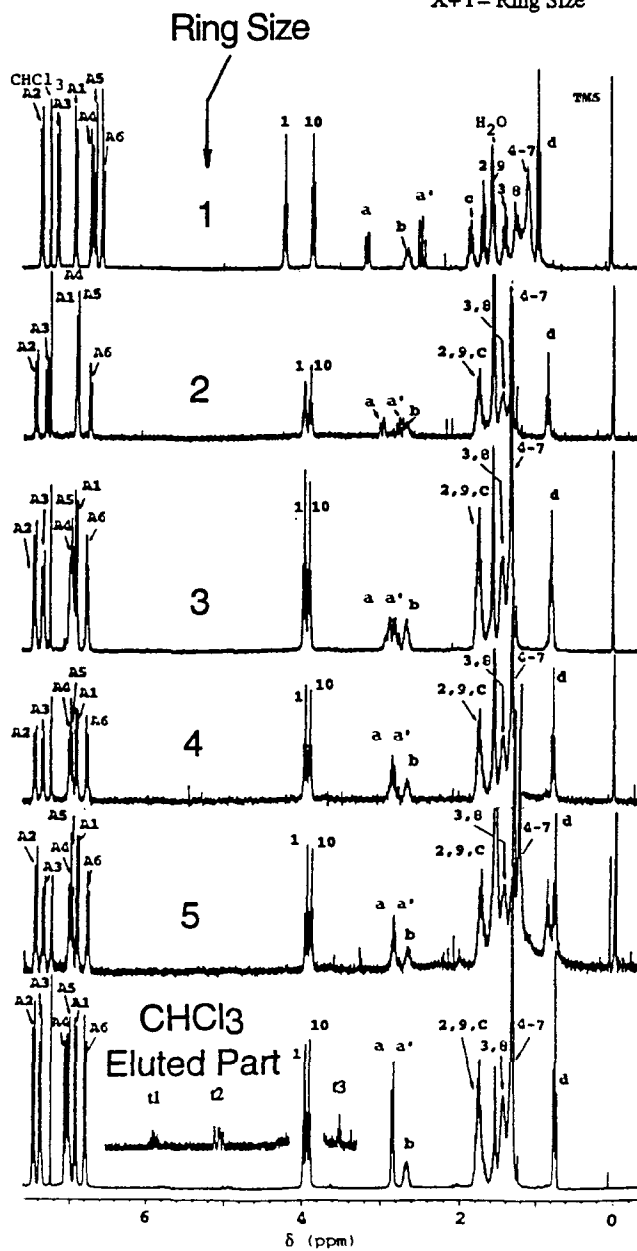
very beginning, and a large variety of structural and dynamic investigations should be performed before a comprehensive understanding of these systems will become available. Nevertheless, even at this stage we foresee a series of new concepts which will emerge from these supramolecular channel-like architectures. For example, preliminary investigations have suggested that they act like supramolecular ionic channels [11]. In these channels the ionic conductivity is absent in the crystalline phase and takes place in the Φ_h and isotropic phases. Electronic channels can be designed via similar principles. The contents of these channels can be released via external regulation either by the use of temperature or solvent. Chemical reactions can be performed on the ion pairs complexed within the channel, and this can open new avenues for nanostructures and catalysis. Polymerization reactions performed within the channels of these supramolecular architectures can generate information about reactions in restricted geometries.

Macrocyclic Liquid Crystals Based on 1-(4-Hydroxy-4′-biphenylyl)-2-(4-hydroxyphenyl)butane and Flexible Spacers

Soon after the discovery of liquid crystals [23a] it was recognized that rigid linear and disklike molecules provide the most suitable molecular architectures which lead to liquid crystalline mesophases [23b]. One hundred years later, the discussion on the molecular structure–properties relationship in the field of liquid crystals is still focused on the same two architectures and on few, less conventional variants of them [23c–j]. The same statement is valid for the field of macromolecular and supramolecular liquid crystals [24].

Recently, we predicted and demonstrated that low-molar-mass macrocyclics based on conformationally flexible rodlike mesogens should and do exhibit a higher ability to generate liquid crystalline phases than do their low-molar-mass linear and both their linear and cyclic high molecular mass homologues [25] (Fig. 14). The trend outlined in Fig. 14 is due to the fact that macrocyclics of a certain size are more rigid than are the corresponding linear homologues as well as both their high molecular mass and linear and cyclic compounds. Therefore, with a proper combination of spacer and mesogenic group lengths and macrocyclic ring size, they should be able to generate a liquid crystalline mesophase with an isotropization temperature higher than that of its corresponding linear low and high molecular weight homologues. At present, we are investigating the macrocyclic oligopolyethers of the conformationally flexible compound 1-(4-hydroxy-4′-biphenylyl)-2-(4-hydroxyphenyl)butane (TPB) with α,ω-dibromoalkanes [25] and comparing their phase behavior with that of the corresponding linear polyethers [26]. Questions like: What is the shortest spacer and the minimum ring size of macrocyclic based on TPB which displays a liquid crystalline phase [25d]?; What is the lowest size of the macrocyclic which displays a liquid crystalline phase whose isotropization temperature is higher than that of its linear high molecular mass homologue [25a, 25d,

---

FIG. 16.   300 MHz ^{1}H-NMR spectra of TPB-$(c)10(z)$ ($z = 1$ to 5 is marked on the spectra as ring size) and of the CHCl$_3$-diluted part which contains high molecular weight linear and macrocyclic polyethers.

25f]?; What is the probability of transforming kinetically prohibited [25b] and/or kinetically controlled [25c] mesophases of the linear polymer into enantiotropic mesophases via cyclization?; and What is the ability to generate noncrystallizable macrocyclics with high glass transition temperature and a broad range of temperature of their mesophase [25e]?; were addressed and answered in previous publications.

Although various classes of cyclic oligomers are generated during both step condensations and ring-opening polymerizations [27], and are also important natural compounds such as ionophores [28], cyclodextrins [28], DNA, and peptides [27], there is very little understanding of the similarities and differences among cyclic and linear oligomers and polymers. This is mostly due to the difficult synthesis of cyclic oligomers [27] and polymers [27]. Previously, cyclic glassy oligomers and polymers, i.e., polystyrene [27, 29], polysiloxanes [27, 30], and poly-(2-vinylpyridine) [31], have been synthesized and characterized. Cyclic oligomers of polycarbonate [32] and of a few other condensation polymers [33] have also been reported. Cyclic oligomers of polyethylene were prepared and used to understand the crystallization mechanism of polyethylene [27, 34], while cyclic side-chain crystalline oligomers and polymers have only recently been reported [35]. Probably the best investigated classes of macrocyclics are crown ethers, cryptands, calixarenes, and other cyclophanes which form host–guest complexes [36]. Recently, interest centered around supramolecular chemistry [36] has generated a great deal of activity in the area of complex architectures based on macrocyclics such as catenanes [37a–c], rotaxanes [37d–f], and knots [37b, 37c]. Macrocyclic liquid crystals are adding a new dimension to this entire field which so far has been concerned with liquid, glassy, and crystalline states.

Figure 15 outlines the synthetic procedure used for the preparation of the macrocyclic and high molecular weight linear polyethers based on TPB and α,ω-dibromoalkanes. For simplicity we will use the same nomenclature for their abbreviations as was used in previous publications [25]. That is, TPB-(l)X refers to the linear (l) polyethers obtained from the racemic TPB and a flexible spacer containing an X number of methylenic units, while TPB-(c)X(z) refers to the cyclic (c) oligoethers based on the racemic TPB, containing an X number of methylenic units and a degree of oligomerization equal to z (i.e., $z = 1$, monomer; $z = 2$, dimer; etc.). Optimum reaction conditions for the synthesis of macrocyclics [25a] and high molecular weight linear [26] polymers based on TPB were elaborated. The individual macrocyclic compounds can be separated by column chromatography, while the low concentration of macrocyclics present in the high molecular weight linear polymers is normally separated by precipitation in acetone (Fig. 15).

The structure of the macrocyclic compounds was demonstrated by a combination of techniques consisting of 300 MHz 1-D ^{1}H-NMR spectroscopies and molecular weight determination [25a]. Aside from the absence of chain ends, a very interesting characteristic of the ^{1}H-NMR spectra of macrocyclic compounds consists of the dependence of some of their resonances on ring size. Figure 16 presents a series of 300 MHz ^{1}H-NMR spectra of TPB-(c)10(z) with $z = 1, 2, 3, 4,$ and 5 and of their high molecular weight fraction which was eluted with CHCl$_3$ from the chromatographic column (Fig. 15). This fraction contains both high molecular weight linear and cyclic compounds. It can be observed clearly from the NMR spectra in Fig. 16, and from the plot of some representative chemical shifts as a
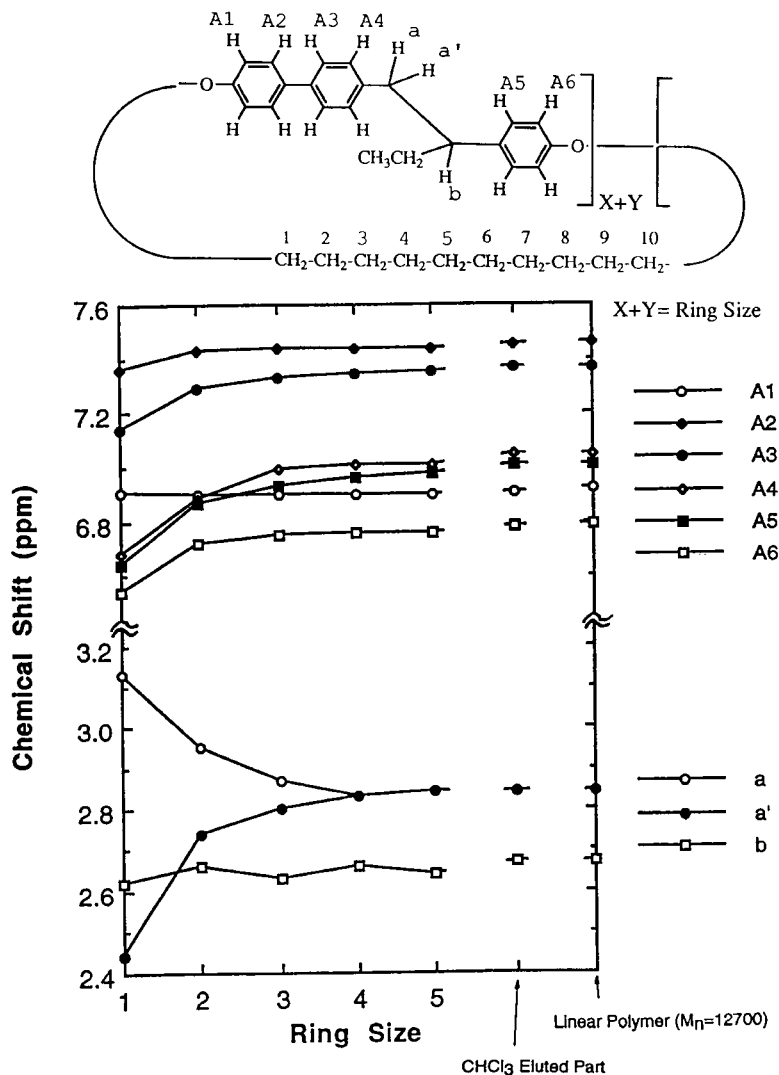
FIG. 17.   The dependence of selected chemical shifts of TPB-$(c)10(z)$ on ring size (z = 1 to 5) and its comparison with the chemical shifts of the high molecular weight macrocyclic and linear polyethers.

function of ring size in Fig. 17, that the chemical shifts of the cyclic compounds are strongly dependent on molecular weight. Chemical shifts of the pentamer start to resemble those of the high molecular weight linear and high molecular weight macrocyclic compounds. The two pairs of chemical shifts that seem to be most relevant are the doublets a and a' and the triplets 1 and 10. For example, in the cyclic monomer the doublets a and a' are separated by about 0.75 ppm, while in high molecular weight structures they became a single doublet. The triplets 1 and 10 are about 0.45 ppm apart in the cyclic monomer and are separated by only 0.1 ppm

Dimer

Trimers

$2L_f' + L_f$: Length to make a fold

L_m : Length of mesogen

L_s : Length of spacer

: Mesogenic Unit
Anti Conformer

: Mesogenic Unit
Gauche Conformer
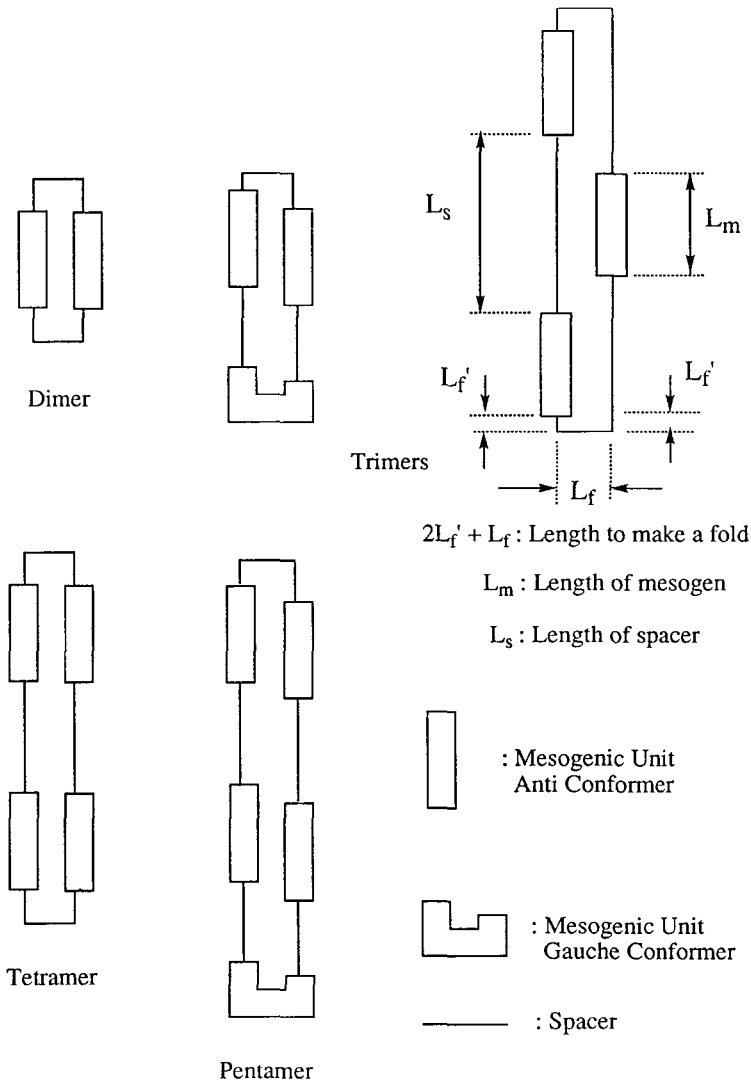
: Spacer

Tetramer

Pentamer

FIG. 18.   The ideal architecture of cyclic oligomers (dimer to pentamer) in the crystalline and liquid crystalline phases.

in the high molecular weight structures. These results suggest that in the case of macrocyclics based on TPB and 1,10-dibromodecane, the ring strain decreases dramatically passing from monomer to pentamer. As was shown in Fig. 15, TPB has two conformational isomers (*anti* and *gauche*). They are both of help during the macrocyclization reaction and also permit various configurational flexibilities to be tolerated in the architecture of a certain macrocyclic compound.

Figure 18 outlines the ideal configurations of the macrocyclic structures which should be tolerated by crystalline and liquid crystalline structures. The cyclic monomer is not included in this figure since the TPB unit is always in its *gauche* con-

Monomer

CH_3—$(CH_2)_9$—O—⬡—⬡—⟨—⬡—O—$(CH_2)_9$—CH_3

Dimers

Trimers

+ Constitutional Isomers

Tetramers

+ Constitutional Isomers
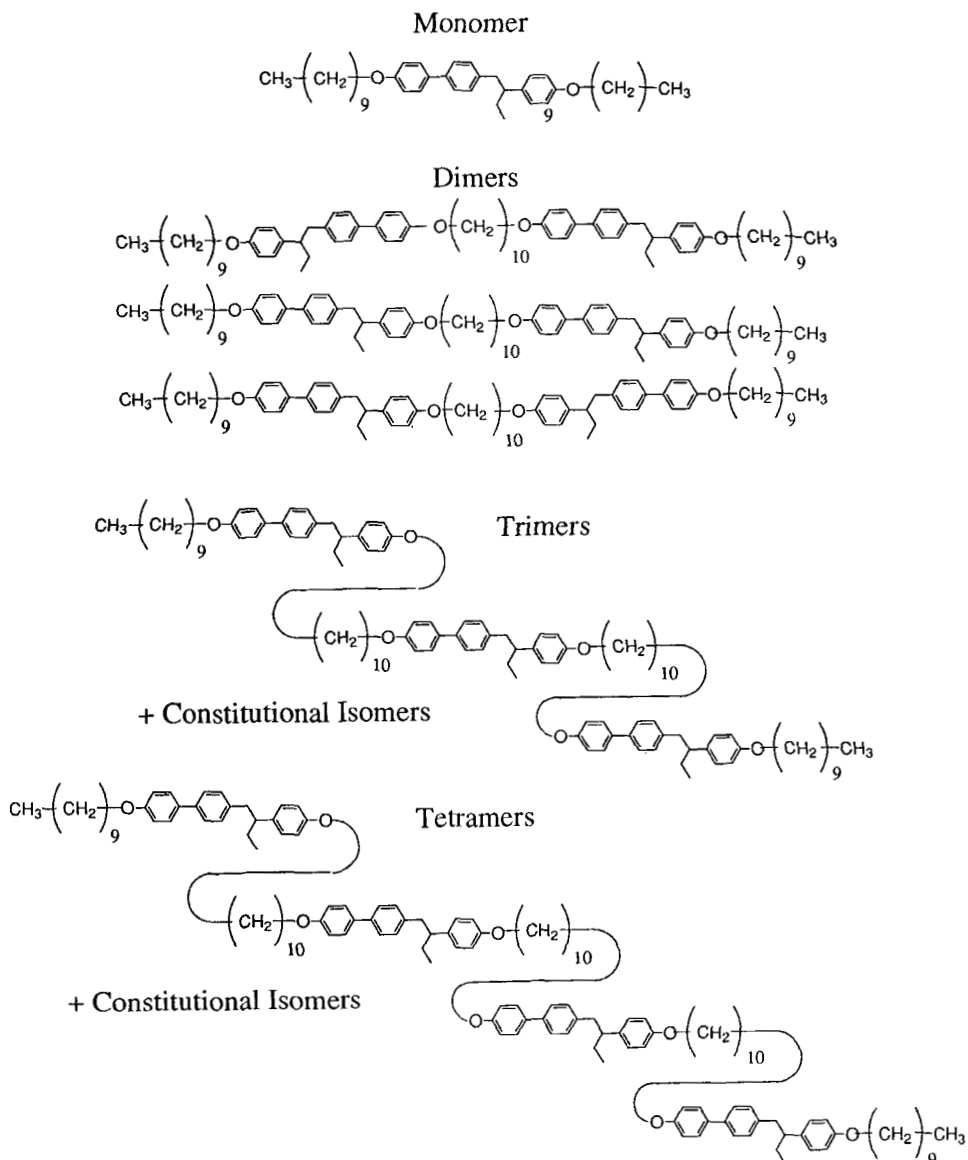
FIG. 19.   The structures of the linear model compounds (monomer to tetramer) of TPB and 1,10-dibromodecane.

former and, therefore, the cyclic monomers are always liquid. However, optimum correlations between the lengths of the spacer and of TPB units should generate collapsed macrocyclics which would have to generate liquid crystalline phases. In order to provide a quantitative comparison between the individual linear model compounds, the monomer, dimer, trimer, tetramer (Fig. 19), and the high molecular weight polymers with narrow molecular weight distribution were synthesized [38].

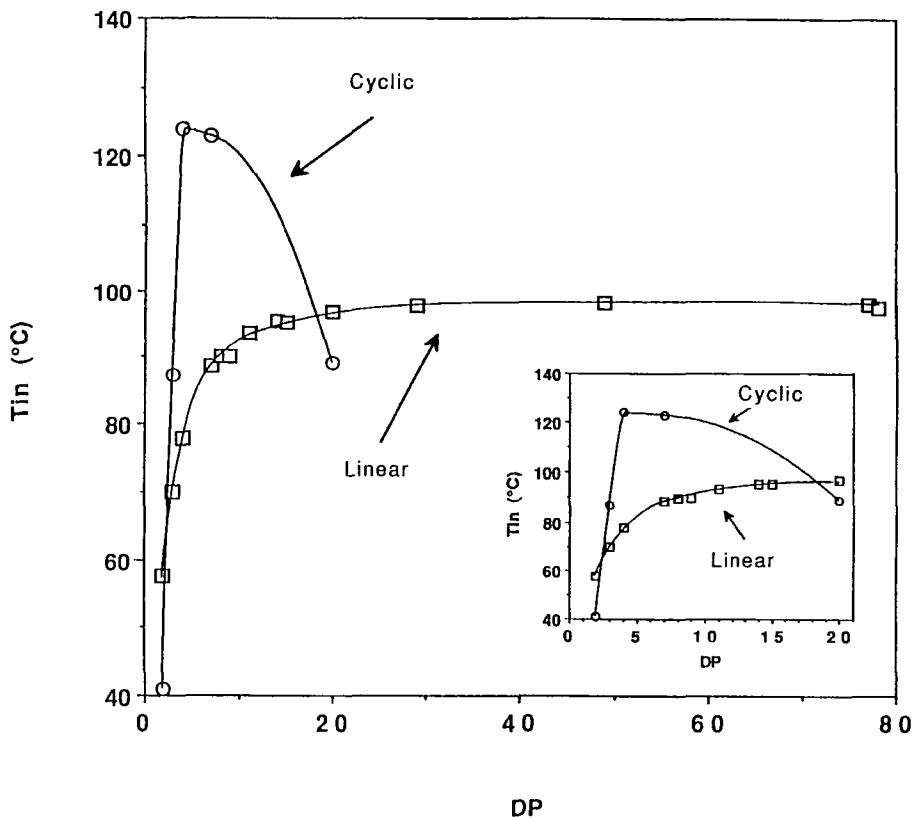FIG. 20.   Dependence of the isotropic–nematic (T_{in}) transition temperatures of linear (□) and macrocyclic (○) TPB oligomers and polymers on their degree of polymerization.

Their phase behavior determined from cooling DSC scans is compared with that of the corresponding cyclic compounds in Fig. 20 [38]. Both linear and cyclic compounds larger than dimer generate a nematic mesophase. The linear dimer has a higher isotropization than the cyclic one. However, the cyclic trimer displays a much higher ability to form the nematic mesophase than the corresponding linear trimer. At the same time, the cyclic tetramer and pentamer exhibit much higher abilities to form nematic mesophases than even the very high molecular weight linear polymers (Fig. 20). These results demonstrate that at least in the core of the macrocyclic compounds based on TPB and 1,10-dibromodecane, the tetramer and pentamer and not the linear high molecular polymers exhibit the highest tendency to form nematic mesophases.

Figure 21 outlines the most probable mechanism for the nematic–isotropic phase transition of the macrocyclic tetramer. In the nematic phase the spacer should form a very tight fold. Mesogen–mesogen intramolecular recognition helps in the generation of this tightly collapsed structure which is more rigid than the corresponding linear counterpart, and therefore, exhibits a higher isotropization temperature. These macrocyclics should display various individual and cooperative motions which are not encountered in conventional linear rodlike nematic mesogens.
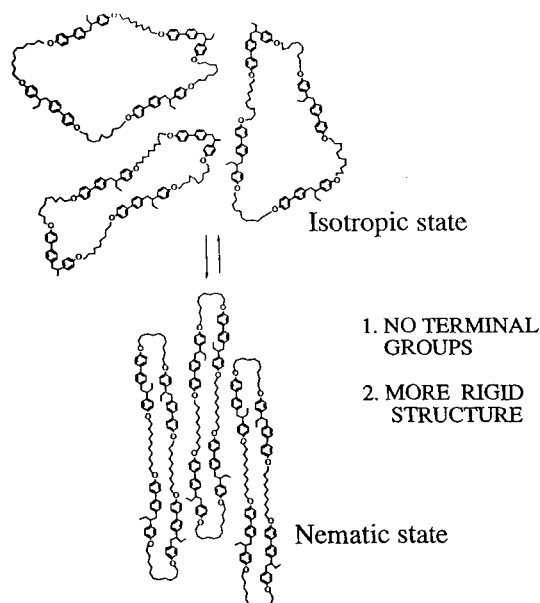
Isotropic state

1. NO TERMINAL
   GROUPS

2. MORE RIGID
   STRUCTURE

Nematic state

FIG. 21.   Schematic representation of the mechanism of the isotropic–nematic transition of TPB-(c)10(4).

A more comprehensive comparison of linear and cyclic molecules of different sizes is presented elsewhere [39].

In this brief discussion we would like to bring the attention of the reader to two more particular sets of data which are summarized in Figs. 22 and 23. Figure 22(a) plots the isotropization temperatures (T_{ni}) of macrocyclic tetramers and of linear polymers as a function of the number of methylenic units in the spacer. As we can see from this figure, both series of compounds display a conventional odd-even dependence which vanishes at long spacers. The only unusual result is that macrocyclic tetramers always have higher isotropization transition temperatures than their corresponding linear polymers. Figure 22(b) plots the enthalpy changes (ΔH_{ni}) associated with the isotropization transition temperatures from Fig. 22(a). ΔH_{ni}s of cyclic tetramers are lower than of the corresponding linear polymers. This is due to the fact that the difference between the entropy of a macrocyclic in its isotropic and nematic phases is lower than the corresponding parameter of a linear polymer. The message generated by Fig. 22 is that cyclic tetramers have both expected similarities and differences with the corresponding linear high molecular weight polymers.

Figure 23(a) plots the phase transition temperatures and Fig. 23(b) the ΔH_{ni} values for the macrocyclic trimers based on TPB as a functions of spacer length. An odd-even dependence of the T_{ni} data is observed. This dependence is completely different from that of the corresponding tetramers and of linear high molecular weight polymers (Fig. 22a). First, T_{ni} shows a very weak odd-even dependence of spacer length. However, this dependence shows a reverse trend with that described in Fig. 22(a). That is, cyclic tetramers and linear high molecular weight polymers exhibit higher T_{ni} for even spacers while cyclic trimers show higher T_{ni} for odd
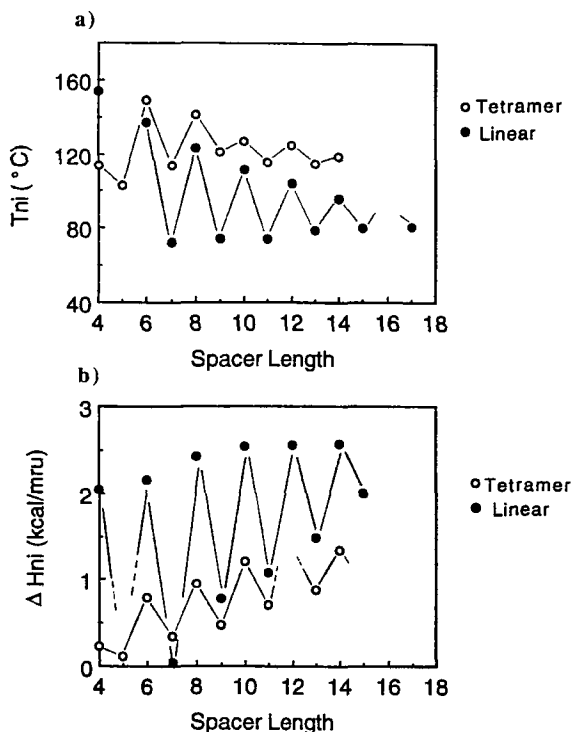
FIG. 22. The dependence of the isotropic–nematic transition temperature (T_{ni}) (a) and of its associated enthalpy changes (ΔH_{ni}) (b) of TPB-(c)X(4) (cyclic tetramer) and TPB-(l)X (high molecular weight linear polymer) on spacer length (X).

spacers. At the same time, T_{ni} of cyclic trimers increases continuously as a function of spacer length (Fig. 23a). This last trend suggests that the rigidity of cyclic trimers increases continuously with their spacer length. This trend was never observed before in low molar mass liquid crystals or in main chain liquid crystalline polymers. This statement is supported by the dependence of ΔH_{ni} versus spacer length (Fig. 23b) which shows a continuous increase. Finally, cyclic trimers with very short and very long spacers exhibit, in addition to the nematic mesophase, a smectic A (S_A) phase. Regardless of the spacer length, the layer of the S_A phase of the cyclic tetrimers is equal to $1.5(L_m + L_s)$ in which L_m is the length of TPB in its *anti*-conformation while L_s is equal to the length of the flexible spacer in its fully extended all-*trans*-conformation (Fig. 18). A S_A mesophase like the one shown on the top right side of Fig. 18 requires that $2L_m + L_s = 2(L_s - 2.5) + L_m$, where 2.5 Å is the minimum length of the 180° turn in the fold which is generated by two carbon atoms. Under these circumstances the shorter spacer length which can accommodate a structure like this should be equal or longer than the length of the mesogen, i.e., $L_s \geq L_m$. Alternatively, at that spacer length a S_A phase can be formed only when one TPB mesogenic group is in its *gauche* conformation and it is part of the fold (middle top structure in Fig. 18). Preliminary experiments with macrocyclics based on enantiomerically-enriched TPB suggest that heterochiral recognition
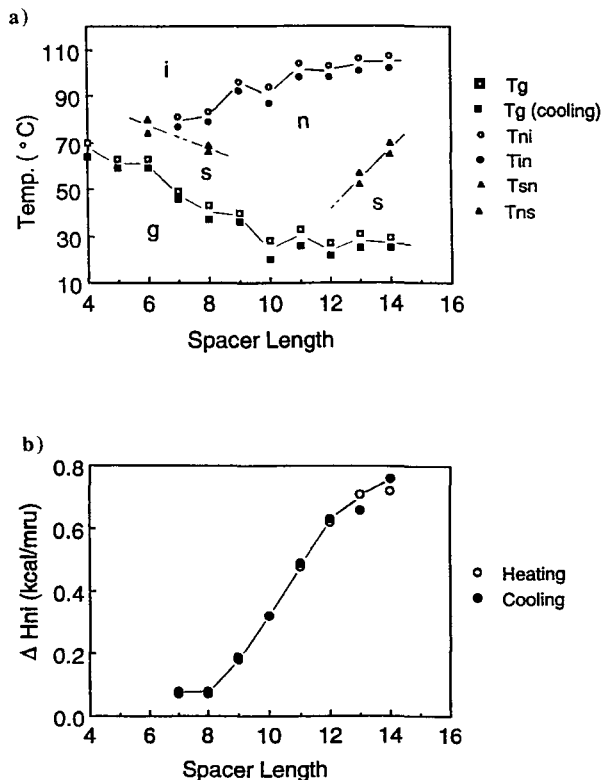
a)

b)

FIG. 23. The dependence of the various transition temperatures (a) and of the enthalpy change (b) associated with the nematic–isotropic (ΔH_{ni}) transition temperatures of TPB-(c)X(3) (cyclic trimer) versus spacer length (X).

between the two enantiomers available in the racemic mixture may make a contribution to the architecture of the macrocyclic in the mesophase [40]. The nematic mesophase exhibited by those macrocyclics is biaxial [41].

This novel class of liquid crystals opens numerous possibilities for the design of new macromolecular and supramolecular architectures based on liquid crystalline macrocyclic building blocks.

ACKNOWLEDGMENTS

REFERENCES

[1] J. M. Lehn, *Angew. Chem., Int. Ed. Engl.*, 27, 89 (1988); (b) D. J. Cram, *Ibid.*, 27, 1009 (1988); (c) C. J. Pedersen, *Ibid.*, 27, 1021 (1988).
[2] (a) J. M. Lehn, *Ibid.*, 29, 1304 (1990); (b) H. J. Schneider, *Ibid.*, 30, 1417 (1991).

[3]   For some brief reviews on self-assembly see: (a) J. S. Lindsey, *New J. Chem.*, *15*, 153 (1991); (b) G. M. Whitesides, J. P. Matthias, and C. T. Seto, *Science*, *254*, 1312 (1991); (c) H. J. Schneider and H. Durr (Eds.), *Frontiers in Supramolecular Organic Chemistry and Photochemistry*, VCH, New York, 1991; (d) J. M. Lehn, *Makromol. Chem., Macromol. Symp.*, *69*, 1 (1993).

[4]   (a) J. Rebek Jr., *Angew. Chem., Int. Ed. Engl.*, *29*, 245 (1990); (b) D. Philp and J. F. Stoddart, *Synlett*, p. 445 (1991).

[5]   A. Klug, *Angew. Chem., Int. Ed. Engl.*, *22*, 565 (1983).

[6]   J. N. Israelachvili, *Intermolecular and Surface Forces*, Academic Press, New York, 1992, p. 380.

[7]   (a) G. H. Brown and J. J. Wolken, *Liquid Crystals and Biological Structures*, Academic Press, New York, 1979, p. 35; (b) V. Degiorgio and M. Corti (Eds.), *Physics of Amphiphiles: Micelles, Vesicles, and Microemulsions*, North-Holland, New York, 1985, p. 7.

[8]   V. Percec, J. Heck, and G. Ungar, *Macromolecules*, *24*, 4597 (1991).

[9]   V. Percec, M. Lee, J. Heck, H. E. Blackwell, G. Ungar, and A. Alvarez-Castillo, *J. Mater. Chem.*, *2*, 931 (1992).

[10]   V. Percec, M. Lee, J. Heck, G. Ungar, and A. Alvarez-Castillo, *J. Mater. Chem.*, *2*, 1033 (1992).

[11]   V. Percec, G. Johansson, J. Heck, G. Ungar, and S. V. Batty, *J. Chem. Soc., Perkin Trans. 1*, p. 1411 (1993).

[12]   G. Johnasson, V. Percec, G. Ungar, and D. Abramic, *Ibid.*, In Press.

[13]   D. M. Dishong, C. J. Diamond, M. I. Cinoman, and G. W. Gokel, *J. Am. Chem. Soc.*, *105*, 586 (1983).

[14]   K. Kikukawa, G. X. He, A. Abe, T. Goto, R. Arata, T. Ikeda, F. Wada, and T. Matsuda, *J. Chem. Soc., Perkin Trans. 2*, p. 135 (1987).

[15]   Y. Takeda, *Top. Curr. Chem.*, *121*, 1 (1984).

[16]   (a) M. A. Bush and M. R. Truter, *J. Chem. Soc., Perkin Trans. 2*, p. 341 (1972); (b) R. Mallinson and M. R. Truter, *Ibid.*, pp. 341, 1818 (1972).

[17]   D. J. Cram, *Angew. Chem., Int. Ed. Engl.*, *25*, 1039 (1986).

[18]   V. Percec, J. Heck, D. Tomazos, F. Falkenberg, H. Blackwell, and G. Ungar, *J. Chem. Soc., Perkin Trans. 1*, p. 2799 (1993).

[19]   V. Percec, J. Heck, D. Tomazos, and G. Ungar, *J. Chem. Soc., Perkin Trans. 2*, p. 2381 (1993).

[20]   V. Percec, D. Tomazos, J. Heck, H. Blackwell, and G. Ungar, *Ibid.*, p. 31 (1994).

[21]   V. Percec, J. Heck, G. Ungar, and D. Abramic, To Be Published.

[22]   D. Tomazos, G. Out, J. Heck, G. Johansson, V. Percec, and M. Möller, *Liq. Cryst.*, *16*, 509 (1994).

[23]   (a) F. Reinitzer, *Monatsh. Chem.*, *9*, 421 (1888). An English translation of this paper was published in *Liq. Cryst.*, *5*, 7 (1989); (b) D. Vorländer, *Z. Phys. Chem.*, *105*, 211 (1923); (c) G. W. Gray, *Molecular Structure and the Properties of Liquid Crystals*, Academic Press, London, 1962; (d) G. R. Luckhurst and G. W. Gray (Eds.), *The Molecular Physics of Liquid Crystals*, Academic Press, London, 1979, p. 14; (e) G. W. Gray, *Philos. Trans. R. Soc. London, Ser. A*, *309*, 77 (1983); (f) G. W. Gray, *Proc. R. Soc. London, Ser. A*, *402*, 1 (1985); (g) H. Kelker and T. Hatz, *Handbook of Liquid Crystals*, Verlag Chemie, Weinheim, 1980; (h) D. Demus and H. Zaschke, *Flussige Kristalle in Tabellen*, VEB Deutscher Verlag für Grundstoffindustrie,

Leipzig, Vol. 2, 1984; (i) D. Demus, *Mol. Cryst. Liq. Cryst*, *165*, 45 (1988); (j) D. Demus, *Liq. Cryst.*, *5*, 75 (1989).

[24] For some recent reviews on macromolecular and supramolecular liquid crystals see: (a) V. Percec and D. Tomazos, "Molecular Engineering of Liquid Crystalline Polymers," in *Comprehensive Polymer Science*, 1st Supplement (Sir Geoffrey Allen, Ed.), Pergamon Press, Oxford, 1992, pp. 300–383; (b) V. Percec and D. Tomazos, "Reactions and Interaction in Liquid Crystalline Media," in *Polymerization in Organized Media* (C. M. Paleos, Ed.), Gordon and Breach, Philadelphia, 1992, pp. 1–104; (c) V. Percec and D. Tomazos, *Adv. Mater.*, *4*, 548 (1992); (d) V. Percec and D. Tomazos, "Recent Developments in Tailor Made Liquid Crystalline Polymers," in *Frontiers in Macromolecular Chemistry*, special issue of *Indian J. Technol.*, *31*, 339–392 (1993); (e) V. Percec and D. Tomazos, "Molecular Engineering of Side Chain LCPs," in *Contemporary Topics in Polymer Science*, Vol. 7, *Advances in New Materials* (J. C. Salamone and J. Riffle, Eds.), Plenum Press, New York, 1992, pp. 247–268; (f) H. Ringsdorf, F. Schlarb, and G. Venzmer, *Angew. Chem., Int. Ed. Engl.*, *27*, 113 (1988).

[25] (a) V. Percec, M. Kawasumi, P. L. Rinaldi, and V. E. Litman, *Macromolecules*, *25*, 3851 (1992); (b) V. Percec and M. Kawasumi, *Adv. Mater.*, *4*, 572 (1992); (c) V. Percec and M. Kawasumi, *Liq. Cryst.*, *13*, 83 (1993); (d) V. Percec and M. Kawasumi, *Mol. Cryst. Liq. Cryst.*, *238*, 21 (1994); (e) V. Percec and M. Kawasumi, *Chem. Mater.*, *5*, 826 (1993); (f) V. Percec and M. Kawasumi, *J. Mater. Chem.*, *3*, 725 (1993).

[26] V. Percec and M. Kawasumi, *Macromolecules*, *24*, 6318 (1991).

[27] (a) V. Percec, C. Pugh, O. Nuyken, and S. D. Pask in *Comprehensive Polymer Science*, Vol. 6 (G. Allen and J. C. Bevington, Eds.), Pergamon Press, Oxford, 1989, p. 281; (b) P. Rempp, C. Strazielle, and P. Lutz in *Encyclopedia of Polymer Science and Engineering*), Vol. 9, 2nd ed. (H. F. Mark, N. M. Bikales, C. G. Overberger, G. Menges, and J. I. Kroschwitz, Eds.), Wiley, New York, 1987, p. 183; (c) *Cyclic Polymers* (J. A. Semlyen, Ed.), Elsevier Applied Science Publishers, New York, 1986; (d) P. Knops, N. Sendhoff, H.-B. Mekelburger, and F. Vögtle, *Top. Curr. Chem.*, *161*, 1 (1991); (e) A. Ostrowicki, E. Koepp, and F. Vögtle, *Ibid.*, *161*, 37 (1991); (f) J. P. Mathias and J. F. Stoddart, *Chem. Soc. Rev.*, *21*, 215 (1992).

[28] (a) R. Hilgenfeld and W. Saenger, *Top. Curr. Chem.*, *101*, 1 (1992); (b) J. F. Stoddart, *Carbohyd. Res.*, *12*, 192 (1989); (c) W. Saenger, *Angew. Chem., Int. Ed. Engl.*, *19*, 344 (1980).

[29] (a) B. Vollmert and J. X. Huang, *Makromol. Chem., Rapid Commun.*, *2*, 467 (1981); (b) D. Geiser and H. Höcker, *Macromolecules*, *13*, 653 (1980); (c) J. Roovers and P. M. Toporowski, *Ibid.*, *16*, 843 (1983); (d) J. Roovers, *Ibid.*, *18*, 1359 (1985); (e) G. Hild, A. Kohler, and P. Rempp, *Eur. Polym. J.*, *16*, 525 (1980); (f) G. Hild, A. Kohler, and P. Rempp., *Ibid.*, *19*, 721 (1983); (g) J. Sundararajan and T. E. Hogen-Esch, *Am. Chem. Soc., Div. Polym. Chem., Polym. Prepr.*, *32*, 604 (1991).

[30] (a) S. J. Clarson and J. A. Semlyen, *Polymer*, *27*, 1633 (1986); (b) S. J. Clarson, K. Dodgson, and J. A. Semlyen, *Ibid.*, *26*, 930 (1985); (c) C. M. Kuo and S. J. Clarson, *Am. Chem. Soc., Div. Polym. Chem., Polym. Prepr.*, *32*, 595 (1991).

[31] (a) J. Sundararajan and T. E. Hogen-Esch, *Am. Chem. Soc., Div. Polym.*

Chem., Polym. Prepr., *32*, 63 (1991); (b) J. Sundararajan and T. E. Hogen-Esch, *Ibid.*, *33*, 162 (1992).

[32] (a) D. J. Brunelle, E. P. Boden, and T. G. Shannon, *J. Am. Chem. Soc.*, *112*, 2399 (1990); (b) D. J. Brunelle and E. P. Boden, *Makromol. Chem.*, *Macromol. Symp.*, *54/55*, 397 (1992) and references cited therein.

[33] (a) H. M. Colquhoun, C. C. Dudman, M. Thomas, C. A. O'Mahoney, and D. J. Williams, *J. Chem. Soc., Chem. Commun.*, p. 336 (1990); (b) M. A. Buese, *Macromolecules*, *23*, 4341 (1990).

[34] M. Möller, R. F. Waldron, J. Drotloff, and D. Emeis, *Polymer*, *28*, 1200 (1987) and references cited therein.

[35] (a) V. Percec and B. Hahn, *J. Polym. Sci., Polym. Chem. Ed.*, *27*, 2367 (1989); (b) R. D. C. Richards, W. D. Hawthorne, J. S. Hill, M. S. White, D. Lacey, J. A. Semlyen, G. W. Gray, and T. C. Kendrick, *J. Chem. Soc., Chem. Commun.*, p. 95 (1990).

[36] For recent reviews and books on various macrocyclics forming host-guest complexes see: (a) F. Vögtle and E. Weber (Eds.), *Host Guest Complex Chemistry, Macrocyclics*, Springer Verlag, New York, 1985; (b) L. F. Lindoy, *The Chemistry of Macrocyclic Ligand Complexes*, Cambridge University Press, Cambridge, 1989; (c) J. M. Lehn, *Angew. Chem., Int. Ed. Engl.*, *27*, 89 (1988); (d) J. M. Lehn, *Ibid.*, *29*, 1304 (1990); (e) C. D. Gutsche, *Calixarenes*, Royal Society of Chemistry, Cambridge, 1989; (f) G. Gokel, *Crown Ethers and Cryptands*, Royal Society of Chemistry, Cambridge, 1991; (g) F. Diederich, *Cyclophanes*, Royal Society of Chemistry, Cambridge, 1991.

[37] For recent reviews on catenands, rotaxanes, and knots see: (a) C. Dietrich-Buchecker and J. P. Sauvage, *Chem. Rev.*, *87*, 795 (1987); (b) J. P. Sauvage, *Acc. Chem. Res.*, *23*, 319 (1990); (c) C. Dietrich-Buchecker and J. P. Sauvage, *New J. Chem.*, *16*, 277 (1992); (d) D. Philp and J. F. Stoddart, *Synlett*, p. 445 (1991); (e) J. F. Stoddart, *Angew. Chem., Int. Ed. Engl.*, *31*, 846 (1992); (f) H. W. Gibson, P. T. Engen, Y. X. Shen, J. Sze, C. Lim, M. Bheda, and C. Wu, *Makromol. Chem., Macromol. Symp.*, *54/55*, 519 (1992).

[38] V. Percec and M. Kawasumi, *Macromolecules*, *26*, 3663 (1993).

[39] V. Percec and M. Kawasumi, *J. Chem. Soc., Perkin Trans. 1*, p. 1319 (1993).

[40] V. Percec and M. Kawasumi, *Macromolecules*, *26*, 3917 (1993).

[41] (a) J. F. Li, V. Percec, and C. Rosenblatt, *Phys. Rev. E.*, *48*, R1 (1993); (b) J. F. Li, V. Percec, C. Rosenblatt, and O. D. Lavrentovich, *Europhys. Lett.*, *25*, 199 (1994).